Using ephaptic coupling to estimate the synaptic cleft resistivity of the calyx of Held synapse.

Short title: **Electronic model of the synaptic cleft.**

Martijn C. Sierksma & J. Gerard G. Borst

Department of Neuroscience, Erasmus MC, University Medical Center Rotterdam, 3000 CA, Rotterdam, The Netherlands.

Correspondence to g.borst@erasmusmc.nl

A conference paper including parts of this paper was presented at Proceedings of the 23rd International Congress on Acoustics (2019, doi: 10.18154/RWTH-CONV-240008)

Keywords: Prespike; Cleft conductance; Giant synapse; Cleft potential; Auditory brainstem.

Abstract

At synapses, the pre- and postsynaptic cell get so close that currents entering the cleft do not flow exclusively along its conductance, g_{cl}. A prominent example is found in the calyx of Held synapse in the medial nucleus of the trapezoid body (MNTB), where the presynaptic action potential can be recorded in the postsynaptic cell in the form of a prespike. Here, we developed a theoretical framework for ephaptic coupling via the synaptic cleft, and we tested its predictions using the MNTB prespike recorded in voltage-clamp. The shape of the prespike is predicted to resemble either the first or the second derivative of the inverted, presynaptic action potential if cleft currents dissipate either mostly capacitively or resistively, respectively. We found that the resistive dissipation scenario provided a better description of the prespike shape. Its size is predicted to scale with the fourth power of the radius of the synapse, explaining why intracellularly recorded prespikes are uncommon in the central nervous system. We show that presynaptic calcium currents also contribute to the prespike shape. This calcium prespike resembled the first derivative of the inverted calcium current, again as predicted by the resistive dissipation scenario. Using this calcium prespike, we obtained an estimate for g_{cl} of ~1 μS. We demonstrate that, for a circular synapse geometry, such as in conventional boutons or the immature calyx of Held, g_{cl} is scale-invariant and only defined by extracellular resistivity, which was ~75 Ωcm, and by cleft height. During development the calyx of Held develops fenestrations. We show that these fenestrations effectively minimize the cleft potentials generated by the adult action potential, which might otherwise interfere with calcium channel opening. We thus provide a quantitative account of the dissipation of currents by the synaptic cleft, which can be readily extrapolated to conventional, bouton-like synapses.

Author Summary

At chemical synapses two neurons are separated by a cleft, which is very narrow. As a result, the concentration of released neurotransmitter can rapidly peak, which is essential for fast synaptic transmission. At the same time, the currents that flow across the membranes that face the synaptic cleft are also substantial, and a fraction of these currents will enter the other cell. We made an electronic model of the synaptic cleft, which indicated that if the shape and fraction of these currents are known, the electrical resistance of the synaptic cleft can be inferred. We tested several of the predictions of our model by comparing the membrane currents during a presynaptic action potential in a giant terminal, the calyx of Held, with the much smaller prespike evoked by these currents in the postsynaptic cell. We estimate the cleft resistance to be about 1 MΩ, which means that the changes in the cleft potential due to the membrane currents can become large enough to have an impact on voltage-dependent calcium channels controlling neurotransmitter release.

Introduction

When sir Sherrington introduced the term 'synapsis' [1], it was still unknown whether or not nerve impulses reach their target through direct electrical coupling [2, 3]. The visualization by electron microscopy of the synaptic cleft, the narrow gap between an axon and its target, put this debate to rest in favor of transmitter-mediated neurotransmission [4-6]. At about the same time, the electrical circuitry of the synapse was outlined, which included a cleft leak conductance (g_{cl}) linking synaptic currents with the interstitial space [7]. Since then, the purported role of the synaptic cleft for synaptic transmission has gradually become more important. Its small volume not only allows a rapid buildup of released neurotransmitter, but protons [8, 9], and potassium ions [10-12] may accumulate as well, whereas calcium ions may become partially depleted [13, 14]. Interestingly, during transmission a cleft potential may arise that may alter the dwelling time of mobile, charged particles within the cleft [15, 16], the distribution of ligand-gated ion channels [17], or the kinetics of voltage-gated channels in the cleft-facing membrane [18]. These features all stem from the small size of the synaptic cleft, which thus forms a barrier for particle movements [19].

Except for some specialized synapses, the contribution of g_{cl} to synaptic transmission has largely been ignored or deemed irrelevant, but its importance will of course depend on its magnitude and on the size of the currents that flow within the cleft. Eccles and Jaeger [7] already indicated that the maximal cleft current will be limited by this conductance. g_{cl} decreases as the path length l_{path} to the extracellular space increases ($g_{cl} \sim A/(R_{ex}\, l_{path})$, where R_{ex} is extracellular resistivity in Ω cm and A the area through which the current flows (see also ref. [20]). Due to their much longer path length, it has been argued that giant synapses have a lower g_{cl} than conventional synapses [21]. Remarkably, estimates of g_{cl} of very different synapses vary over four orders of magnitude (range 1.4 nS to 40 μS) without a clear relation to synapse size [7, 11, 18, 20, 22-30]. Despite the remarkable progress in our understanding of the synaptic cleft, we need a better theoretical understanding of its conductive properties, which is ideally confirmed by experimental observations.

One of the largest synapses in the mammalian brain is the calyx of Held synapse, which spans about 25 µm [31, 32]. Its large size matches its strength, with the maximal glutamatergic conductance exceeding 100 nS, and its fast presynaptic AP allowing firing rates >300 Hz [33]. Large currents, related to the excitatory postsynaptic current (EPSC) and capacitive currents, need to flow within the cleft through g_{cl}, and under these conditions g_{cl} may limit synaptic transmission. A characteristic feature of this synapse is that the presynaptic AP can be detected in the postsynaptic recording (Figure 1). This hallmark of the calyx of Held synapse has been called the prespike [34]. It is probably due to ephaptic coupling of the presynaptic AP via the synaptic cleft [30, 35], but the precise relation between the presynaptic AP and the prespike has not been studied analytically. Here, we use the prespike to infer some key electrical properties of this giant synapse. We provide a theoretical description of ephaptic coupling by defining the electrical properties of the synaptic cleft, which is validated through dual patch-clamp recordings of the calyx of Held and its postsynaptic target.

Results

The prespike is the ephaptically coupled calyx of Held AP recorded in its target neuron, a principal neuron in the medial nucleus of the trapezoid body (MNTB) [34]. Some current clamp (CC) and voltage clamp (VC) prespike examples are shown in Figure 1A-B. Figure 1C shows that the amplitudes of the CC and the VC prespikes recorded in the same cell are correlated. Figure 1D shows examples of the CC prespikes recorded during *in vivo* whole-cell recordings in young rats, whose shape resemble those recorded in the simultaneous pre- and postsynaptic slice recordings (Figure 1A-B, 2A).

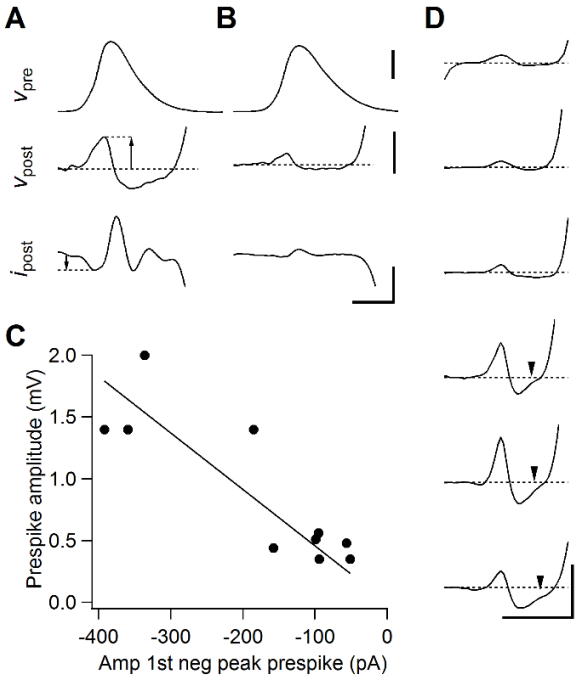

Figure 1 – Examples of prespikes. (A-B) Two examples of prespikes in simultaneous pre- and postsynaptic patch-clamp recordings. From top to bottom: calyx of Held AP, which was elicited by afferent stimulation, CC prespike, associated VC prespike. Recordings were made at room temperature in brainstem slices from 7-10 days old Wistar rats [36]. Horizontal scale bar: 0.5 ms. Vertical (from top to bottom): 50 mV, 2 mV, 1 nA. Arrows indicate the amplitudes that were quantified in (C). (C) Relation between amplitude of the positive peak of the prespike measured in CC and the amplitude of the first negative peak of the prespike measured in VC in the same cell. Slope of the fitted line is -4.6 mV/nA. (D). Six examples of CC prespikes from *in vivo* recordings of a target neuron of the calyx of Held in 3-5 days old Wistar rats [37]. During this period the calyx

of Held expands over the postsynaptic cell. Note the small upward deflection immediately preceding the EPSP in the bottom three prespikes (arrow heads). Scale bar indicates 0.5 mV and 0.5 ms.

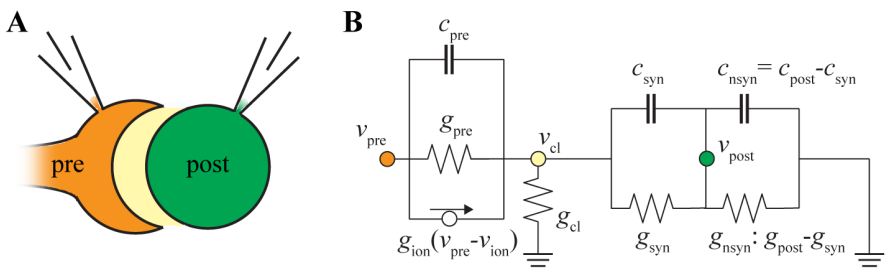

Figure 2. An electrical circuit for the prespike. (A) Drawing of the calyx of Held synapse. The calyx of Held terminal ('pre') covers a large part of the soma of its target neuron ('post'). In between is the synaptic cleft (not drawn to scale), a small space where membrane currents will flow during a presynaptic AP. (B) Electrical circuit to reproduce the prespike. Presynaptic membrane currents can leave the synaptic cleft via the cleft conductance (g_{cl}) or through the postsynaptic cell. It is assumed that the conductance from the edge of the cleft to ground is relatively large compared to the cleft conductance itself [38, 39].

The prespike: a dissipation of cleft currents.

The prespike is generated by currents that flow from the calyx to the principal neuron in the MNTB. While the current flow through the cleft depends on the synapse geometry, which we will consider later in this article, we can already get a good understanding by analyzing a prespike-generating, electrical circuit, similar to ref. [30], with the following components (Figure 2B): (1) the terminal's release face, consisting of voltage-gated conductances, a capacitor (c_{pre}), and a conductance (g_{pre}); (2) the synaptic cleft, which is separated from the reference by a leak conductance (g_{cl}), and (3) a passive neuron, which partly faces the synaptic cleft. This part consists of a capacitor (c_{syn}) and a leak conductance (g_{syn}). The remainder of the postsynaptic cell consists of a capacitor (c_{nsyn}=c_{post}-c_{syn}) and a leak conductance (g_{nsyn}=g_{post}-g_{syn}). As the prespike is small, we ignore the postsynaptic voltage-dependent conductances. We also did not include a direct resistive

connection between calyx and target since there is no physiological evidence for gap junctions at the calyx of Held synapse [40], and capacitive currents are likely to dominate the electrical coupling: the susceptance at 1 kHz across an area of 1000 μm^2 is 63 nS ($2\pi f C_m A$, where f is the frequency, C_m is the specific capacitance, and A the membrane area), which is much larger than the postsynaptic resting conductance of ~4 nS.

Using Kirchhoff's law of current conservation ($i_{leave} = i_{enter}$), we define the equation for v_{cl} and subsequently the equations for the prespike (see Appendix A1 for the derivations). The equation for v_{cl} is $v_{cl}(g_{cl} + \sum g_{ion}) + (c_{pre} + c_{syn})dv_{cl}/dt = c_{pre}dv_{pre}/dt + \sum g_{ion}(v_{pre} - v_{ion})$. The right-hand side shows the currents entering the cleft (i_{enter}), which are the presynaptic capacitive current and the currents through the voltage-dependent ion channels. The left-hand side of the equation shows the currents leaving the cleft (i_{leave}), which are generated by the cleft potential. This response will lie between two extremes: (1) the capacitive dissipation scenario, where the cleft poses a high resistance, resistive currents can be neglected, and the currents that leave the cleft are capacitive-only, and (2) the resistive dissipation scenario where the cleft is highly conductive, and the currents that leave the cleft are entirely resistive. For the capacitive dissipation scenario, we derive that $v_{cl} = v_{constant} + (c_{pre} + c_{syn})^{-1} \int i_{enter} dt$; and v_{cl} then resembles scaled, integrated i_{enter}, and therefore a scaled, presynaptic AP and the integrated voltage-gated currents. For the resistive dissipation scenario, we derive in Appendix A that $v_{cl} = i_{enter}(g_{cl})^{-1}$; v_{cl} will then resemble a scaled i_{enter}, which therefore should resemble the first derivative of the presynaptic AP.

The VC prespike represents the capacitive currents over the cleft-facing postsynaptic capacitance. In CC, the prespike currents will change the postsynaptic membrane potential. The equations for the currents entering and leaving the postsynaptic cell are $-i_{rec} = c_{syn}dv_{cl}/dt$ and $c_{post}dv_{post}/dt + g_{post}v_{post} = -i_{rec}$, respectively. The shape of the VC prespike is entirely determined by the shape of dv_{cl}/dt. We can derive how the VC prespike relates to i_{enter} for the two extreme scenarios for the v_{cl}, For the capacitive dissipation scenario, we obtain $-i_{rec} =$

$c_{syn}(c_{pre} + c_{syn})^{-1} i_{enter}$, and therefore the VC prespike resembles the cleft currents scaled by the postsynaptic cleft-facing capacitance relative to the entire cleft-facing capacitance (Appendix A). Due to the giant size of the calyx of Held synapse, the presynaptic and postsynaptic capacitance facing the cleft are close to equal (c_{syn}=c_{pre}=c_{cl}) [41, 42]. This means that: $-i_{rec} = 0.5\ i_{enter}$,and the other 'half' of i_{enter} returns through the presynaptic membrane. (In other words, v_{cl} reduces the capacitive currents from the presynaptic AP (c_{pre} d(v_{pre}-v_{cl})/dt) by half, which dissipate capacitively to the postsynaptic neuron.) For the resistive dissipation scenario, we obtain $-i_{rec} = c_{syn}(g_{cl})^{-1} di_{enter}/dt$. Under these conditions, the VC prespike resembles the (inverted) second derivative of the presynaptic AP scaled by the constant $c_{syn}c_{pre}/g_{cl}$, which for the calyx of Held becomes c_{cl}^2/g_{cl}. We therefore conclude that if the VC prespike resembles the (inverted) first derivative of the presynaptic AP, it indicates that cleft resistance is high, whereas if it resembles the (inverted) second derivative of the presynaptic AP it indicates a relatively low cleft resistance.

Does the VC prespike resemble the first or second derivative of the presynaptic AP? We analyzed simultaneous whole-cell presynaptic current clamp recordings with postsynaptic voltage clamp recordings [36, 43]. In these recordings, the afferent axon of the calyx of Held was stimulated with an electrode to trigger a train of presynaptic APs, and the postsynaptic responses were recorded simultaneously (Figure 3A). The prespike generally matched the scaled, inverted second derivative of the AP (Figure 3B), taking into account that it may have been filtered by the series resistance. Figure 3C shows that the time course of the second derivative of the AP indeed provides a better match for the prespike than its first derivative (n = 13 paired recordings). This is in agreement with the idea that the cleft currents mainly dissipate resistively. During the train, the presynaptic AP becomes smaller and slower [36, 44], resulting in a substantial reduction in the presynaptic capacitive current amplitudes. To investigate the impact of these changes on the prespike, we plotted the first two peaks of the prespike against the first two peaks of the first or the second derivative (Figure 3D). In each case, the second derivative of the presynaptic AP gave a better fit

(Figure 3D-E, AP' versus AP''): Pearson's r = -0.967 ± 0.018 vs. -0.979 ± 0.018, paired T-test, t_{12} = 5.4, p = 0.00017). Furthermore, this fit should cross through the origin, since either $-i_{post} = g_{cl}\tau_{cl}{}^2 d^2 v_{pre}/dt$ or $i_{post} = 0.5\, c_{pre}\, dv_{pre}/dt$ for the resistive dissipation or the capacitive dissipation scenarios, respectively. The absolute deviation for the second derivative at 0 V/s^2 was significantly less for every recording than for the first derivative at 0 V/s (Figure 3F, AP' versus AP''): deviation = 122 ± 145 pA versus 20 ± 37 pA, paired T-test, t_{12} = 3.3, p = 0.0060). These fits also yielded an estimate for $g_{cl}\tau_{cl}^2$, namely the slope from the fit of the second derivative and the prespike amplitudes, which was 0.11 ± 0.07 fA s^2 V^{-1} (Figure 3G). These observations are thus in agreement with the prespike resembling the inverted second derivative of the presynaptic AP, suggesting that the cleft currents mostly dissipate through the cleft conductance.

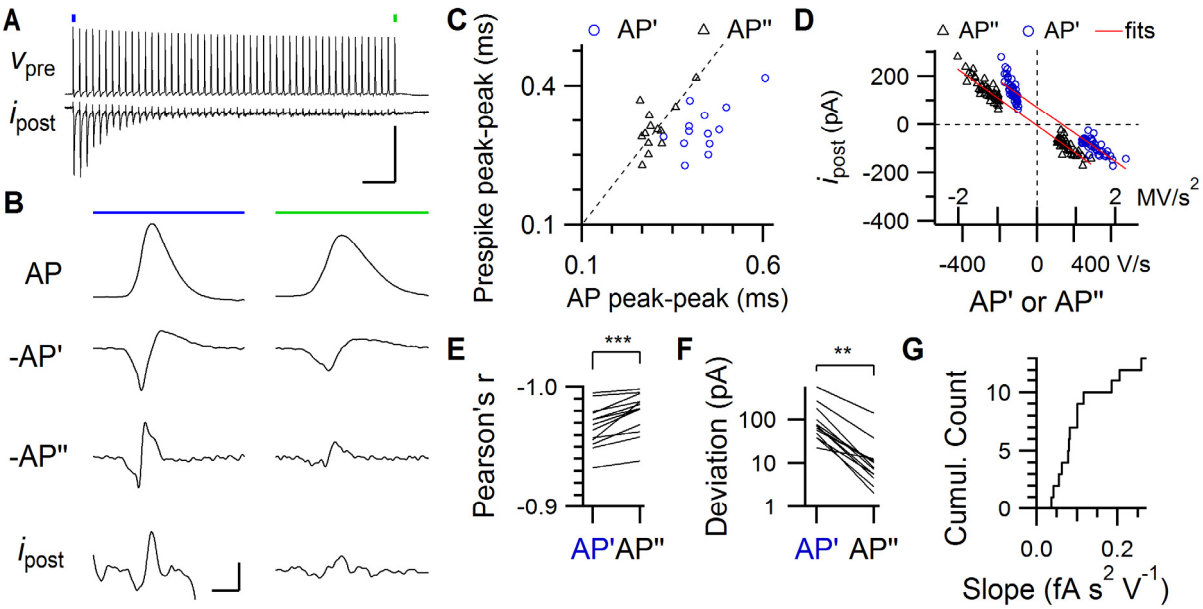

Figure 3 – Relation between the calyceal AP and the prespike. (A) An example of a train of presynaptic APs (v_{pre}) elicited by afferent stimulation and the postsynaptic voltage-clamp recording (i_{post}). A large EPSC is elicited by the first AP, which rapidly depresses during the train. Stimulation artefacts were blanked. The first AP (blue dot) and the last AP (green dot) are shown on an expanded scale in B. Horizontal scale bar: 50 ms. Vertical scale bar: 90 mV, 1.5 nA. (B) The left and right column show the first and last AP of the train,

respectively. *From top to bottom*: the AP recorded in CC from the calyx of Held, its inverted first (-AP') and second derivative (-AP''), and postsynaptic voltage clamp recording showing the accompanying prespike (i_{post}). Vertical scale bars (from top to bottom panels): 40 mV, 0.3 kV/s, 2.5 MV/s^2, 0.2 nA. Horizontal: 0.5 ms. (C) Relation between the delay between the first negative and positive peak of the prespike and the first two peaks in the first (blue, circle) and second (black, triangle) derivative of the presynaptic AP of the first AP-prespike pair in the train. Dashed line is the identity line. (D) Relation between the amplitude between the first negative and positive peak of the prespike and the first two peaks in the first (blue, circle) and second (black, triangle) derivative of the presynaptic AP of all AP-prespike pairs from an example train. The red lines indicate the linear regression lines. Note how the regression line crosses closer to the origin for the second derivative than for the first derivative. (E) Comparison for each train of Pearson's *r* for the regression lines. (F) Comparison of the absolute deviation at 0 V/s (AP') versus 0 V/s^2 (AP''). (G) Cumulative distribution of the regression slope. Paired T-tests: ** $p<0.01$, *** $p<0.001$.

The calcium prespike

Voltage-gated currents inside the cleft also contribute to v_{cl}. We explored how the presynaptic calcium current would affect the prespike (Appendix 1.2 for the derivations). As the prespike depends on the current entering the cleft i_{enter} irrespective of the origin of the current, a voltage-dependent calcium current in the cleft should also contribute to the prespike. We call the part of the VC prespike that is determined by the cleft calcium current, the calcium prespike. For the capacitive dissipation scenario, we expect that the calcium prespike is $-i_{rec} = i_{ca}$. (Here, i_{ca} is defined as the recorded current at the presynaptic terminal which is the net current through the calcium channels and the cleft-facing capacitance, and by definition, this current dissipates across the postsynaptic membrane.) For the resistive dissipation scenario, the calcium prespike is $-i_{rec} = c_{syn}(g_{cl})^{-1} di_{ca}/dt$. Note that c_{cl}/g_{cl} equals a time constant, which we call the cleft time constant $\tau_{cl}=c_{cl}/g_{cl}$. We can write $-i_{rec} = \tau_{cl}\, di_{ca}/dt$. The calcium prespike will either resemble an inverted

calcium current, or an inverted, scaled first derivative of the calcium current.

We turned to simultaneous pre- and postsynaptic whole-cell voltage clamp recordings of the calyx of Held synapse that were originally reported in ref. [44], which were used to evaluate the presence or absence of a calcium prespike. In these experiments the presynaptic compartment was voltage clamped with an action potential waveform (APW) command while the presynaptic calcium currents were pharmacologically isolated (Figure 4A). To isolate the calcium prespike from the recorded prespike, we averaged the postsynaptic responses to the P/5 AP waveforms and subtracted the upscaled, passive prespike from the 'active' prespike. The remaining currents indeed resembled the first derivative of the calcium current (Appendix A4; Figure 4A-B, Figure S1), confirming not only the existence of a calcium prespike, but also that its shape is in agreement with the cleft currents dissipating through the different, resistive routes.

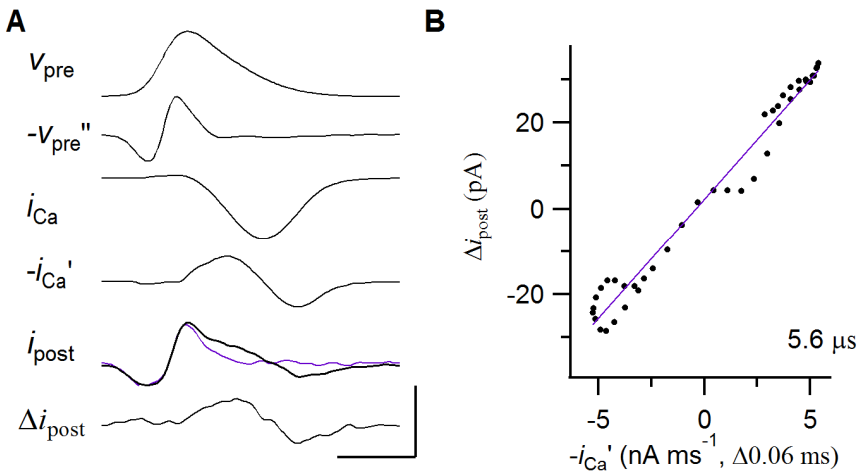

Figure 4 – Relation between the calcium current and the prespike. (A) *from top to bottom*: The presynaptic voltage-clamp waveform (v_{pre}), the inverted second derivative of the waveform ($-v_{pre}''$), the presynaptic calcium current (i_{Ca}; after P/5 subtraction), its inverted first derivative ($-i_{Ca}'$), the active (black, thick) and passive prespike (i_{post}; magenta, P/5-scaled), and the calcium prespike which is the difference between the active and the passive prespike (Δi_{post}). The passive prespike is generated by injecting the presynaptic AP at 1/5th of its amplitude. While this generates passive currents across the presynaptic cleft-facing membrane, it does not elicit the presynaptic calcium current. Voltage-gated sodium and potassium currents were blocked (see Methods).

Vertical scale bars: 110 mV, 7 MV/s^2, 2 nA, 15 nA/ms, 0.15 nA, 0.1 nA. Horizontal: 0.5 ms. (B) Relation between the inverted first derivative of the presynaptic calcium current and the calcium prespike (black dots). Maximum correlation was obtained by introducing a delay of 60 µs for the first derivative. The slope of the regression line (magenta) is shown in the bottom right corner.

From the analytical derivations for the resistive dissipation scenario, we know that the presynaptic calcium current and the calcium prespike are related by the cleft time constant τ_{cl}. To estimate τ_{cl}, we first analyzed the presynaptic calcium current that was evoked by the APW. It had a peak amplitude of -1.9 ± 0.6 nA and a full-width at half-maximum (FWHM) of 0.51 ± 0.05 ms (n = 5 paired recordings). Next, we obtained the values for the calcium prespike. Its peak-to-peak amplitude was 80 ± 60 pA and its peak-to-peak delay was 0.54 ± 0.11 ms. This peak-to-peak delay should be about twice τ_{Ca}, which was thus slightly higher than the 0.21 ms reported in ref. [45]. Its time course closely matched our prediction for the resistive dissipation scenario (Figure 4, Appendix A2, Figure S1). The amplitude of the calcium current was linearly related to the calcium prespike peak (r = 0.98, p = 0.003); the calcium prespike peak was 1.9 ± 0.7% of the calcium current amplitude. In Appendix A2 we derived that this percentage should be $\tau_{cl}\ \tau_{Ca}^{-1}e^{-0.5}$, yielding an estimated τ_{cl} of 9 ± 5 µs. As an alternative approach, we plot the first derivative of the presynaptic calcium current against the calcium prespike. Its maximal slope (allowing for a slight time shift) provided a τ_{cl} of 5.7 ± 1.9 µs (Figure 4B and 9B). The two methods thus gave comparable values for the cleft time constant.

The ratio of cleft capacitance c_{cl} and cleft leak conductance g_{cl} constitutes τ_{cl}. If we assume that c_{cl} is in the order of 10 pF, the estimated g_{cl} becomes about 0.5-1 µS. From the circuit analysis we know that the capacitive VC coming from both the presynaptic AP and the calcium prespike from the presynaptic calcium current do not scale the same way to c_{cl} and g_{cl} (*cf.* Appendix A1 with A2). This difference allows us to further define these two parameters. From the calcium prespike we

obtain τ_{cl}. As the equation for the capacitive prespike can be written as $-i_{post} = g_{cl}\tau_{cl}{}^2 d^2 v_{pre}/dt$, we find that we can calculate g_{cl}. The first peak of the VC prespike had an amplitude of -120 ± 110 pA, which corresponds to the capacitive currents. We can then calculate a g_{cl} of 2.6 ± 0.8 µS and a c_{cl} of 24 ± 16 pF.

For τ_{cl} we assumed that the calcium current entirely originated from the membrane facing the cleft. These estimates should be considered as a lower bound as some of the current may not arise from the cleft-facing membrane. Immunolabeling for calcium channels identified a fraction of the N-type and R-type calcium channels to be in the non-cleft-facing membrane [46]. If we assume that only two-third of the calcium current originated from the cleft, our estimate of τ_{cl} increases to 13.5 ± 7.8 µs. This estimate could be considered as an upper bound, as less than 50% of the calcium current was mediated by N-type and R-type channels, and the other, P/Q-type, calcium channels were mostly associated with the release face [46]. When we assume that 2/3 of the total presynaptic calcium current originated from the cleft, we calculate a g_{cl} of 1.2 ± 0.4 µS and a c_{cl} of 16 ± 11 pF. With these values $g_{cl}\,\tau_{cl}^2$ was 0.07, 0.08, 0.11, 0.28 and 0.82 fA s^2 V^{-1} (0.27 ± 0.32 fA s^2 V^{-1}), which is in agreement with Figure 3G. Based on our limited data set, we determine that g_{cl} ranges between 1-2 µS.

No evidence for a potassium or a sodium prespike

Besides the capacitive currents and the voltage-gated calcium channels, other voltage-gated channels facing the cleft may also contribute to the cleft currents. We therefore explored the potential contribution of Na^+ and K^+ currents to the prespike, the sodium and potassium prespike, respectively. We estimated their density based on literature values, and assumed a homogeneous distribution within the terminal. As voltage-gated channels in the cleft-facing membrane sense v_{pre}-v_{cl} instead of v_{pre}, their gating depends on v_{cl}. This feedback effect of v_{cl} could not be incorporated in our calculations. Instead, we therefore simulated the impact of voltage-gated currents on the

prespike by numerically solving ordinary differential equations. Figure 5 illustrates that the presence of these channels at the release face may have a large impact on the shape and size of the prespike. Due to the differences in their gating properties, the timing of each current during the presynaptic AP is quite different (Figure 5A), and the same holds for their impact on v_{cl} and on the prespike (Figure 5B). The prespike examples shown in Figure 1 did not resemble the prespike of the homogeneous model, which included Na^+, K^+ and Ca^{2+} currents at the cleft-facing membrane, suggesting that some voltage-gated ion channels are excluded (at least functionally) from the release face. In particular, the voltage-gated sodium conductance generated a current that partially counteracted the first prespike peak. Such rapid changes in the prespike during the rising phase of the presynaptic AP would point at a contribution by sodium channels. However, consistent with previous observations that the terminal is mostly devoid of sodium channels [47-49], these fast changes were not observed in the prespike. We therefore conclude that there is no substantial contribution of sodium channels at the release face to the prespike.

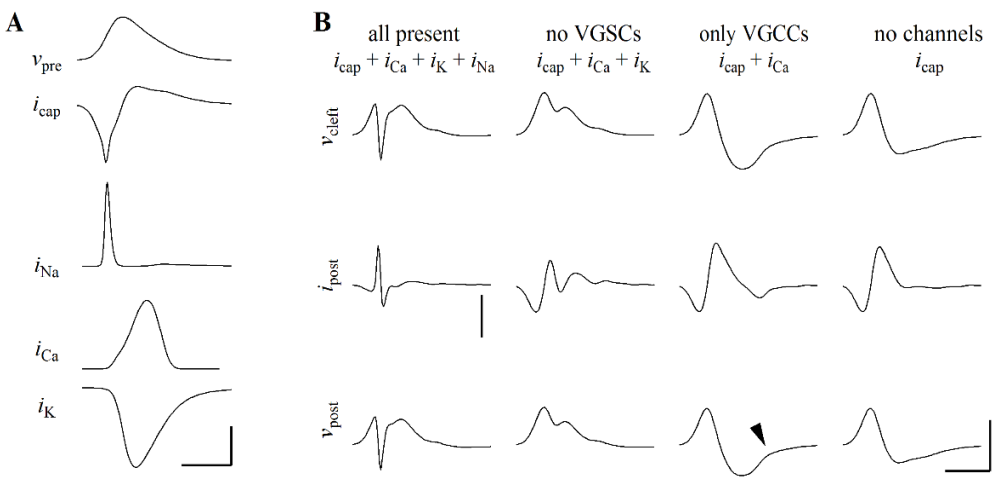

Figure 5 – Impact on the prespike of voltage-gated ion channels located at the release face. (A) Timing of different voltage-gated currents at the release face during the AP. Note that the amplitudes of each of the currents depend on cleft potential, thus creating a mutual dependency. Vertical scale bar: 60 mV, 2.4 nA, 1 nA, 1 nA, 3 nA. Horizontal: 0.5 ms. (B) The cleft potential (top), the VC prespike (middle), and the CC prespike (bottom) in the presence or absence of different voltage-dependent ion channels at the cleft. All present:

homogeneous density for each channel; no VGSCs: no sodium conductance at the release face; only VGCCs: both calcium and capacitive currents at the release face; no channels: the capacitive-only model. The conductances that are present in the model are indicated by their currents at the top. Arrow head indicates the small deflection in the CC prespike that is generated by the calcium prespike. Scale bars: 4 mV, 0.2 nA, 2 mV.; 0.5 ms, except for the homogeneous model where the vertical scale bar corresponds to 1.6 nA.

Potassium channels do not start to open until around the peak of the presynaptic AP. They therefore do not impact the first part of the VC/CC prespike. The potassium current would contribute to a more positive synaptic cleft potential, which is opposite to the effect of the calcium current. If the potassium current at the cleft were significantly larger than the other currents, we would expect a fast inward current in the VC prespike after the first positive peak, and the CC prespike would become a single positive deflection. However, CC prespikes are typically biphasic (Figure 1), therefore the contribution of the potassium current is unlikely to outweigh the contribution of the other currents.

Lastly, we revisit the impact of calcium channels on the prespike. The observation of a calcium prespike already demonstrated the presence of these channels at the release face. The calcium current occurs during the repolarization phase of the presynaptic AP [45], and therefore contributes little to the first two peaks of the VC or to the first peak of the CC prespike. Its contribution is easily obscured by noise or by the EPSC, which starts rapidly after the calcium-induced glutamate release. Nevertheless, it may generate a small, upward inflection in the CC prespike (Figure 5B) and such an inflection can sometimes be observed (Figure 1D).

These simulations show that the prespike waveform may contain information about the presence of voltage-dependent ion channels at the presynaptic membrane facing the cleft. This means that an experimental study of the impact of specific channel blockers on the prespike waveform may be informative about their presence at the release face.

Voltage-dependent kinetics of cleft-facing calcium channels

During development the presynaptic AP narrows from a half width of 0.5 to 0.2 ms [50]. The briefer AP necessitates a much larger capacitive current, which, all else being equal, would generate a larger change in v_{cl}, which may impact the calcium channel kinetics. We again simulated the impact of v_{cl} on the calcium current by solving ordinary differential equations for different values for g_{cl} (Figure 6). For a slow AP, a g_{cl} of 0.67 µS and a c_{cl} of 10 pF, v_{cl} first rises to a maximum of +3.9 mV, and then decreases to a minimum of -4.2 mV. While v_{cl} has little effect on the current amplitude (Figure 6B), it generates a delay of 45 µs in the onset of the calcium current (Figure 6C). In contrast, under the same conditions we observe for a fast AP that v_{cl} rises to a maximum of +16.4 mV, followed by a decrease to a minimum of -8.2 mV. As a consequence, the peak calcium current was delayed by 21 µs and reduced by 19% (-2.0 nA vs -1.7 nA). These effects became even more pronounced at lower g_{cl}. The observed delay corresponded to the delay in reaching the transmembrane $v_{pre} - v_{cleft}$ maximum compared to the v_{pre} maximum; the reduction in calcium current was due to a smaller effective AP, which reduced the maximal open probability of the calcium channels. We conclude that developmental acceleration of the calyceal AP will increase the capacitive current to a level that potentially could delay and impede the presynaptic calcium current substantially if g_{cl} were <1 µS.

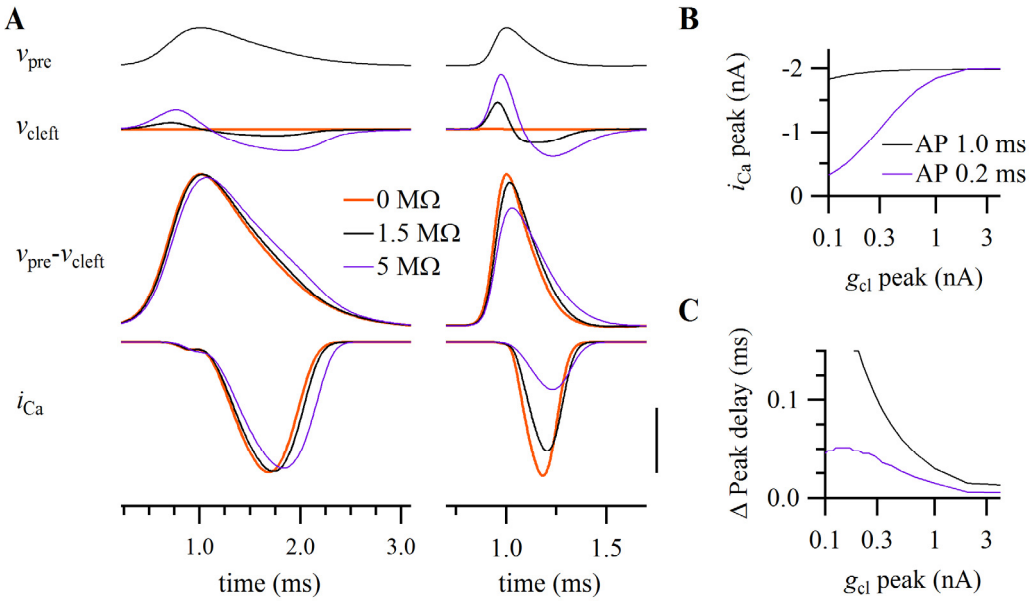

Figure 6 – Potential impact of the cleft potential on presynaptic calcium currents. (A) Simulation of the impact of a slow and a fast AP (top; FWHM: left 1.0, right 0.2 ms) on the cleft potential (second row), the transmembrane potential sensed by the calcium channels in the cleft (third row) and the presynaptic calcium current (bottom) at three leak resistances ($1/g_{cl}$: 0 MΩ, 1 MΩ and 5 MΩ). Scale bar: 200 mV, 40 mV, 50 mV, 1 nA. (B) Relation between peak calcium currents and leak resistance for the two APs. Driving force slightly increases (not shown). (C) The change in delay between the calcium peak current and the AP for the two APs (solid line). The dashed line shows the delay after correcting for the decrease in the calcium current shown in B. Calcium conductance density was adjusted to 0.2 nS μm^{-2} and 2.8 nS μm^{-2} for the slow and fast AP, respectively, in order to elicit a 2 nA-current at 0 MΩ cleft leak resistance. The apposition area was 1000 μm^2. Other conductances were set to 0 nS.

Relation between synapse and prespike size

So far, we modeled the cleft as a single, equipotential compartment with capacitive and conductive properties. However, it is expected that the voltage profile within the cleft will depend on synapse geometry [20], and that larger synapses have larger prespikes [30].We therefore need an analytical

353 description of the voltage profile within the cleft. Previous work considered the impact of cleft geometry
354 on the EPSC, a current that runs radially through the cleft and enters at a centered region containing the
355 glutamate receptors [7, 20, 30]. Our situation is different as we consider a homogeneously distributed
356 current: the capacitive currents arise at every membrane patch facing the cleft. For an analytical
357 description we start by assuming a radially-symmetric synapse with a radius r and a cleft height h. Within
358 this synapse we only consider capacitive currents from the cleft-facing membrane (Figure 7A). As only a
359 small fraction of these currents enters the postsynaptic cell (the resistive dissipation scenario), we simply
360 assume that all currents run radially to the synaptic membranes. The electric field at location x relative to
361 the cleft center will be $dv_{cl}/dx = xR_{ex}C_m(2h)^{-1}dv_{pre}/dt$ (Appendix B1.3) where R_{ex} is the
362 extracellular cleft resistivity and C_m is the specific membrane capacitance. The electric field grows
363 linearly with the distance from the center. The cleft potential is equal to $\int_x^r dv_{cl}\, dx$, which gives $v_{cl} =$
364 $(r^2 - x^2)R_{ex}C_m(4h)^{-1}dv_{pre}/dt$ (Appendix B1.4). The size of the cleft potential thus depends on r^2,
365 indicating that for larger terminals the cleft potential may become increasingly important (Figure 7B). The
366 voltage profile also shows that not all voltage-gated channels in the cleft will be affected, but only the
367 channels located towards the cleft center.

368 The temporal changes in the cleft potential will generate a capacitive current at the postsynaptic side. To
369 obtain the VC prespike, we derive $i_{post} = r^4\pi R_{ex}C_m^2(8h)^{-1}d^2v_{pre}/dt^2$ (Appendix B2.2). The VC
370 prespike therefore grows with the fourth power of the radius, which explains why prespikes are only
371 observed in giant synapses such as the calyx of Held synapse. With our geometrical relation for the VC
372 prespike we can relate g_{cl} to extracellular resistivity: $g_{cl} = 8\pi h(R_{ex})^{-1}$ (Appendix B3). This relation
373 leads to an estimate for the intra-cleft resistivity of 75 Ω cm for an h of 30 nm [41] and a g_{cl} of 1 μS.
374 Considering that there may be extended extracellular spaces within the synaptic cleft [51], and taking into
375 account the variation in g_{cl} (1-2 μS), we estimate an R_{ex} in the range of 50-100 Ω cm.

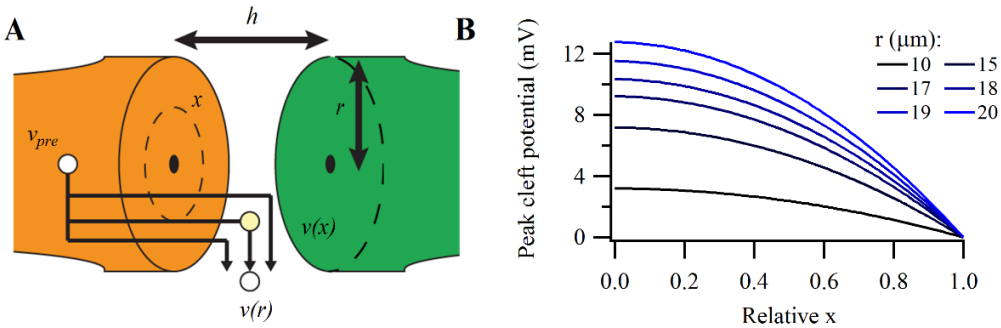

Figure 7. Synapse geometry determines the profile of the cleft potential. (A) Drawing of a radially-symmetric synapse with cleft height *h* and radius *r*. The capacitive currents will generate a cleft potential v(x) at location x. (B) Cleft voltage profile for synapses with different radii (color-coded) at the first peak in the capacitive current. The horizontal axis depicts the location from the center (0) relative to the edge (1.0). In (B), R_{ex} is 100 Ω cm, C_m is 1 µF cm^{-2}, and h is 30 nm.

Fenestration of the calyx of Held reduces cleft potentials.

Giant synapses typically fenestrate during development [52-55]. The relation between fenestration and the coupling between pre- and postsynaptic membranes has been studied in numerical simulations [30]. We initially assumed that fenestration minimizes v_{cl} by reducing g_{cl} through reducing the path length to the extracellular fluid (*r*). However, we analytically derived that for a radially-symmetric synapse, g_{cl} does not depend on its radius. The relation between the conductance and the resistivity is $g_{cl} \sim A\ (r\ R_{ex})^{-1}$, where *A* is the area through which the current escapes. As *A* of a radially-symmetric cleft is $2\pi rh$, when *r* is doubled, *A* is also doubled, leaving the conductance independent of synapse size. The cup-shape of the young calyx makes the radially-symmetric synapse a reasonable approximation. This also means that our estimate of the resistivity of the synaptic cleft is relevant for smaller synapses with a comparable radially-symmetric shape.

Following a period of fenestration, the calyx of Held becomes, as its name implies, a synapse with extended fingers [31, 56]. However, for finger-like synapses with a sheet-like or cylindrical cleft, the geometrical relations are slightly different. For these synapses we assume that the currents only run

396 transversally, *i.e.* perpendicular to the longitudinal axis. The cleft potential then becomes $v(x) =$
397 $(r^2 - x^2)(2h)^{-1} R_{ex} C_m dv_{pre}/dt$ (Appendix B4.4), where $2r$ equals the width of the sheet (or r the length
398 of the cylinder). As the escape route for the current is more restricted than for a radially-symmetric
399 synapse, its voltage gradient is steeper. However, the diameter of a calyceal finger will be much less than
400 the diameter of the juvenile calyx, effectively reducing the cleft potential. For a calyceal finger of 4 μm
401 diameter [31, 57] the cleft potential at the center of the finger-like synapse would be only ~2.5% of the
402 cleft potential in the cup-shape calyceal synapse (equation B5.2). As a consequence, the VC prespike
403 would become ~3.3% assuming that the total contact surface is conserved (equation B5.4). The cleft
404 potential and VC prespike with more complex synapse morphology may be investigated using finite-
405 element modeling, but this is beyond the scope of this study.

406 Fenestration will effectively reduce the amplitude of the cleft potentials, and therefore we expect that the
407 prespike in the adult calyx of Held synapse should be significantly smaller than the juvenile prespike. To
408 study the adult prespike, we revisited *in vivo* whole-cell current-clamp recordings of MNTB principal
409 neurons from wild-type C57BL/6J mice previously reported in refs. [58, 59]. CC prespikes consisted of a
410 small positive deflection, preceding the start of the rapid rising phase of the EPSP by about 0.3 ms. In 11
411 of 12 recordings, the amplitude of the positive deflection was <0.2 mV. In contrast to the juvenile
412 recordings (Figure 1), the positive peak was not followed by a negative peak. An example is shown in
413 Figure 8. The good correlation between the size of CC and VC prespikes (Figure 1C) in combination with
414 the absence of a large decrease in the input resistance of adult principal neurons [58, 59] suggests that the
415 VC prespike can be expected to also be relatively small. Our anecdotal evidence from *in vivo* whole-cell
416 recordings in adult mice therefore confirms that the prespike is smaller than the juvenile prespike and that
417 it possibly has a different shape (*cf.* Figure 1 and 8).

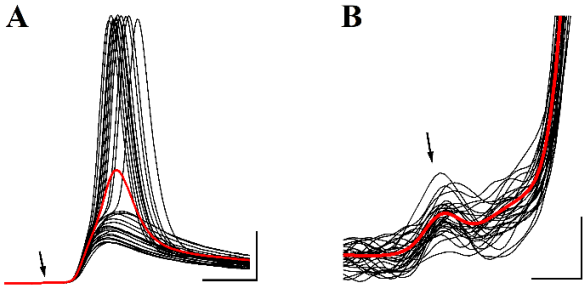

Figure 8 – Adult prespike. (A) Black traces: Spontaneous, sub- and suprathreshold events recorded during a whole-cell *in vivo* recording of a principal neuron in the MNTB from a P52 C57BL/6J mouse [58]. Events were aligned on the start of their EPSP and (<1 mV) differences in the resting membrane potential between events were subtracted for the display. Minimum interval between events was 20 ms. Red trace: average of >1000 events. Resting potential was -64 mV. Arrow points at the small prespike. Vertical scale bar: 10 mV. Horizontal: 1 ms. (B) As (A), showing close-up of the prespike (arrow). Vertical scale bar: 0.2 mV. Horizontal: 0.2 ms.

Discussion

Here, we studied how electrical currents that are needed to depolarize a presynaptic terminal or trigger transmitter release are dissipated in the synaptic cleft. We derived equations for the ephaptic coupling between the presynaptic terminal and the postsynaptic cell. We found that the capacitive component of the prespike is closely approximated by the second time derivative of the presynaptic action potential. Its size scales with the fourth power of the radius of the synapse, explaining why intracellularly recorded prespikes are uncommon in the CNS. We showed that presynaptic calcium currents can contribute to the prespike and that their contribution is closely approximated by the scaled first derivative of these currents. We used their contribution to infer an estimate of the cleft conductance, which was ~1 μS for the juvenile calyx of Held synapse. We showed that the cleft conductance of a radially-symmetric synapse does not depend on its radius, but is entirely defined by its height and the extracellular resistivity. This led to an estimate of the cleft resistivity that is at most 50% larger than of the interstitial fluid, which means that the cleft conductance is large enough to allow for the large EPSCs of the calyx of Held, but small enough to have a potential impact on the opening of presynaptic voltage-dependent calcium channels. Finally, we showed that developmental fenestration of the calyx of Held constitutes a very effective adaptation to minimize synaptic cleft potentials.

Electrical properties of the calyx of Held synapse

Based on our electronic model, we discriminated two extreme scenarios, a scenario in which currents entering the cleft dissipate via the membrane capacitance, and one in which they exclusively dissipate via the cleft conductances. We compared the shape of both the passive and the calcium component of the prespike with both scenarios, and found that the resistive dissipation scenario provided a much better prediction for the shape of the prespike, since the passive prespike resembled the inverted, second derivative of the presynaptic AP much better than the inverted, first derivative, whereas the calcium prespike resembled the inverted, first derivative of the presynaptic calcium currents much better than the

450 inverted calcium currents themselves. There are several other compelling arguments for this scenario. For
451 the calyx of Held synapse to be able to function as a relay synapse in the auditory system, it needs to be
452 both fast and precise, which means a fast presynaptic AP and a large size with many release sites and large
453 EPSCs. We derived for the capacitive dissipation scenario that the size of the prespike would be about half
454 of the size of the presynaptic currents entering the cleft during the presynaptic AP. Because of the large
455 size of the calyx of Held and the fast time course of the presynaptic AP, these currents are in the nA range.
456 The observed size of the VC prespike is therefore clearly not in line with the predictions of the capacitive
457 dissipation scenario. Secondly, the calyceal EPSC is very fast and can easily be 10 nA [36, 50, 60-62].
458 This EPSC should flow not only through the postsynaptic glutamate receptor channels, but also through g_{cl}
459 [7]. For the synapse to be able to conduct an EPSC of 10 nA at a driving force of 100 mV, the cleft leak
460 conductance must be at least >0.1 μS. This is consistent with the observed range for g_{cl}. These arguments
461 are therefore in line with our conclusion that the resistive dissipation scenario provides a much better
462 description than the capacitive dissipation scenario. Less obviously, the model allowed us to use the
463 calcium component of the prespike to obtain an estimate of the cleft conductance of about 1 μS. This
464 value is subject to some uncertainty. For the calculation we assumed that most, but not all, presynaptic
465 calcium channels are facing the synaptic cleft. The juvenile calyx contains N- and R-channels, which are
466 not located near the release sites based on immunostaining and their lower efficacy at triggering release,
467 which is in contrast to the P/Q-type calcium channels [46]. Our assumption that only two-third of the
468 calcium current originated from the cleft is therefore reasonable, considering that the N- and R-channels
469 make up about half of the calcium currents of the juvenile calyx.

470 Even though we calculated the AP-related capacitive currents that run through the cleft-facing membrane,
471 we did not record the AP itself at the cleft-facing membrane. The AP passively invades the terminal [47],
472 and therefore may be slowed down and have a reduced amplitude at the cleft-facing membrane. We
473 consider it unlikely that this filtering is significant for two reasons. First, passive filtering from one end to
474 the other end of the calyx reduces the AP peak by only 6 mV with a delay of <0.2 ms [63]. Second, the

475 axonal AP is able to invade the fenestrated endings of the mature calyx [64], which should have a
476 significantly higher impedance than the cup-shaped calyx. Our calculation of the presynaptic capacitive
477 currents as the rate of change of the recorded calyceal AP relative to the cleft potential is therefore likely
478 to be accurate.

479

480 **Comparison of cleft electrical properties across synapses**

481 Interestingly, with similar values for cleft height and extracellular resistivity other studies came to a wide
482 range of estimated values for the cleft conductance, both at least an order of magnitude smaller than 1 μS
483 [11, 26, 28-30, 65], but in some cases also considerably larger than 1 μS [7, 66]. In some of the synapses,
484 an unusually large and narrow path to the interstitial fluid was responsible for the low estimates. Examples
485 are mossy fiber boutons penetrated by a thin (<1 μm) spinule [28], the unusually long calyx-type
486 vestibular synapse [11], or the cone-to-horizontal cell synapse, for which a large part of the horizontal cell
487 is located within an invagination of the cone photoreceptors [67]. While cleft resistivity should be
488 independent of morphology, the cleft conductance for membrane currents at the deep end of these
489 synapses would be significantly less than for the homogeneously distributed current addressed here. In
490 these morphologically complex synapses, slow removal of ions or neurotransmitter may serve a function,
491 for example in the case of vestibular hair cells, where potassium ions accumulate [10, 11], or in the cone
492 photoreceptor synapse, where prolonged effects of glutamate are important, and where postsynaptic
493 currents are typically relatively small [68]. At the other end of the range lies the high estimate for the cleft
494 conductance of the neuromuscular junction, to which the postjunctional folds were suggested to contribute
495 [7]. The unique morphological properties of these synapses have therefore made a large contribution to the
496 large range of estimated values for the cleft conductance.

497 Our calculations indicated that for homogeneously-distributed currents the associated cleft conductance is
498 fully determined by the extracellular resistivity, the cleft height and the morphological type of the synapse,

but not by the size of the synapse. The cleft height is constrained within narrow boundaries because of the opposing requirements of low volume for high neurotransmitter concentrations and high conductance to allow large synaptic currents [16]. The cleft height typically ranges across synapses between 10-30 nm, but there is some uncertainty regarding the impact of chemical fixation. Assuming a cleft height of 30 nm, we estimated a resistivity of 75 Ω cm based on the prespike, only about 30% larger than of cerebrospinal fluid or Ringer solution [16, 69]. While we are not aware of other estimates of the extracellular resistivity within the synaptic cleft, our estimate is similar to the intracellular resistivity of neurons [70-72] and the periaxonal resistivity of myelinated axons [72]. The extracellular resistivity can also be estimated based on the diffusional mobility of small molecules. Our estimate agrees with those made with an imaging method in hippocampal mossy fiber synapses, which also estimated that small molecules move on average about 50% slower than in the Ringer solution [73]. Estimates of neurotransmitter diffusion constants within the synaptic cleft range from 1.5 to 4 times smaller than in free solution [74-76], but for neurotransmitters diffusion within the synaptic cleft may be slowed down by neurotransmitter-binding proteins. We therefore suggest that a cleft resistivity of ~75 Ω cm may apply to other synapses as well. Given the range of cleft heights and the estimated cleft resistivity, the cleft conductance can be inferred for a distributed current using our analytical relations (B3.2). It should be not so different from the calyx of Held considering that cleft height is conserved across synapses, while the geometry of the juvenile calyx translates well to bouton synapses by simple downscaling. Cleft conductances for circular synapses would then range between 0.3-1.0 μS.

The prespike: what is it good for?

The extracellular AP of the calyx of Held can be observed in extracellular recordings at the target neuron [77], and the characteristic shape of the complex waveform consisting of the presynaptic AP, the EPSP and the postsynaptic AP has facilitated identification of *in vivo* single unit recordings at the MNTB [59]. Importantly, it was shown that the calyceal AP can be picked up in postsynaptic whole-cell recordings as

524 well [34]. This extracellular field potential outside the cleft cannot generate a 0.1 nA-prespike amplitude
525 intracellularly without assuming an obviously non-physiological postsynaptic admittance (~0.2 μS).
526 Incidentally, this also indicates that other compartments, such as the presynaptic heminode, contribute
527 very little to the generation of the prespike. In postsynaptic voltage clamp recordings the prespike showed
528 a resemblance to a high-pass filtered version of the presynaptic AP [36], but we showed here that it is
529 closer to the second derivative of the AP. At the related endbulb of Held synapse, the presynaptic AP is
530 also readily picked up in extracellular recordings [78]. However, no prespikes were reported during
531 postsynaptic whole-cell recordings [79] possibly due to the smaller size of the endbulb compared to the
532 calyx of Held. In the visual system, prespikes can be seen in a subset of lateral geniculate neurons [80].
533 However, in many synapses in which the presynaptic AP is readily observed in extracellular recordings, it
534 is not reported in intracellular postsynaptic recordings [18, 81-85], attesting to the efficiency of the
535 synaptic cleft in dissipating these currents. Interestingly, especially in the hippocampus, neurons can
536 display so-called spikelets with an amplitude of mV in intracellular recordings. They have a biphasic
537 shape resembling the calyceal prespike recorded in current-clamp. These spikelets are thought to result
538 from ephaptic, capacitive coupling with one or more nearby neurons [86]. The equations we derived here
539 should be applicable to these spikelets as well: we predict them to resemble the second derivative of the
540 AP in the nearby neurons [87], and to critically depend on contact area, but also on proximity and on the
541 resistivity of the extracellular fluid.

542 We believe that the major reason for the lack of prespikes at most synapses is that the prespike amplitude
543 is proportional to the 4th power of the synapse radius (Appendix B2). During the postnatal development of
544 the MNTB, it can therefore be argued that the absence of postsynaptic recordings with multiple prespikes
545 cannot be used as firm evidence against the presence of multiple calyces on these cells. We previously
546 found anecdotal evidence for the presence of multiple large inputs during early postnatal development
547 [88]. In a small fraction of the recordings multiple large inputs were observed, one with and one without a
548 prespike. It might be that the one without the prespike had a smaller surface area or a higher cleft height,

549 going below the radar. This highly nonlinear dependence on apposition area may thus provide an
550 explanation for the discrepancy between anatomical evidence favoring multiple large inputs during
551 development [89] and the lack of recordings with multiple prespikes.

552

553 **Divide and conquer**

554 Virtually all synapses have in common that neurotransmission is initiated by a presynaptic action potential
555 that results in capacitive cleft currents. The size of these currents depends on the amplitude and speed of
556 the presynaptic AP. The properties of the presynaptic APs have mostly been studied at giant synapses,
557 where they tend to be large and fast [50, 90-95]. These giant synapses are typically relay synapses that are
558 specialized for rapid signaling, but recent measurements at more conventional bouton synapses in the
559 neocortex show that their presynaptic action potentials are large and fast as well [96]. These capacitive
560 currents, together with the presynaptic ion channel currents, will lead to a change in the cleft potential
561 whose time course will closely follow the time course of the presynaptic membrane currents, and whose
562 amplitude will critically depend on the cleft resistivity. Because of this cleft potential, the presynaptic ion
563 channels facing the cleft will sense a reduced action potential. We showed that this should result in a less
564 effective and delayed opening of the presynaptic calcium channels facing the synaptic cleft. Since rapid
565 and large changes in the voltage sensed by the presynaptic ion channels serve to rapidly turn transmitter
566 release on and off again, large cleft potentials seem undesirable, even though they may serve other, more
567 beneficial functions such as influencing the neurotransmitter mobility within the cleft [15, 16], or rapidly
568 inhibiting postsynaptic action potential generation [18, 97].

569 Above, we argued that many radial-like synapses should have a cleft conductance similar to what was
570 measured here. An important difference between small and large synapses, however, is that the total
571 current will be much larger in the large synapse, as the capacitive current scales with the presynaptic
572 apposition area. A large synapse thus has to dissipate this much larger current over a cleft conductance

573 that is similar to the cleft conductance of a small synapse. There are three obvious different neural
574 strategies to mitigate significant cleft potentials. Firstly, a strategy may be widenings of the synaptic cleft
575 in between synaptic junctions. These intrasynaptic space enlargements [4], also called channels of
576 extracellular spaces [98, 99] or subsynaptic cavities [100], have been found at many synapses, including
577 the calyx of Held synapse, and may increase cleft conductance. Interestingly, a knockout of brevican, a
578 component of the extracellular matrix of perineuronal nets, leads to a reduction of the size of the
579 subsynaptic cavities at the calyx of Held synapse and an increased synaptic delay, even though the relation
580 with a change in cleft conductance remains to be established [100]. The second strategy is to divide the
581 cleft membrane currents over many postsynaptic junctions. For example, in the case of the squid giant
582 synapse, the postsynaptic axon has numerous processes contacting the presynaptic axon, each with a width
583 that is only ~1 μm [101]. At each of these processes the cleft potential will be small, thus effectively
584 mitigating its impact. The last strategy is to fenestrate presynaptically. Most large synapses fenestrate
585 presynaptically during development, leading to extended extracellular spaces [99]. Well-known examples
586 include the neuromuscular junction, where the terminal arbor assumes a pretzel shape [102], the calyx of
587 Held, which develops from a cup shape to the calyx shape [52, 53], the endbulb of Held synapse [54] or
588 the avian ciliary ganglion [55]. In Appendix B5 we quantified the impact this will have on the size of the
589 cleft potential change and on the prespike. Previously, other roles for these adaptations have been
590 emphasized, such as speeding up of transmitter clearance or minimization of crosstalk between
591 postsynaptic densities, both for the calyx of Held synapse [52, 103, 104] and at other synapses [105, 106].
592 The digitated adult morphology of the calyx of Held is accompanied by an increase in the number of
593 puncta adhaerentia [104] and the formation of swellings connected via necks to the fingers [42, 51]. In the
594 adult calyx of Held, a large fraction of the release takes place at these swellings, which should facilitate
595 the dissipation of capacitive currents by the cleft, and reduce the impact of the cleft conductance on the
596 postsynaptic currents.

In conclusion, we show here that the prespike of the calyx of Held synapse can be used to infer critical properties of its synaptic cleft; apart from the cleft conductance, it may also provide information about the presence or absence of ion channels at the cleft, or the effectiveness of morphological changes in reducing the size of cleft potentials during development. We thus provide a quantitative description for how the synaptic cleft, despite its narrow, limited space, can sustain the large and fast currents that are at the heart of chemical neurotransmission.

603 **Materials & Methods**

604 The AP template shown in Figure 4A was based on an AP template previously used in voltage-clamp
605 experiments [43].

606 For the experimental procedures and recording conditions for the dual recordings of the calcium current
607 and the postsynaptic currents, we refer the reader to the original paper in which these recordings were
608 reported [44]. For the current paper, we used trains of 45-50 identical APWs at an interval of 100 Hz.
609 These APWs were what was called the 'control AP' in ref. [44], i.e. the first AP of a train of presynaptic
610 APs. To limit the possible impact of EPSCs on the prespike during the trains, the first 20 APWs were
611 skipped, and the responses to only the next 25 APWs were averaged. The presynaptic passive (capacitive)
612 component was estimated by presenting the same train five times at 5x smaller amplitude, and summing
613 the responses (P/5 method). The capacitive component of the prespike was isolated analogously from the
614 same reduced APW train. *In vivo* whole-cell current-clamp recordings of developing MNTB principal
615 neurons with afferent stimulation were previously reported in ref. [37] (n = 6). *In vivo* whole-cell current-
616 clamp recordings of MNTB principal neurons from adult C57BL/6J mice were previously reported in ref.
617 [58] (n = 7, only wild-type animals) or in ref. [59] (n = 5). We also refer to these papers for the respective
618 ethics statements.

619 For numerical simulations with voltage-gated channels the following two differential equations were
620 defined, following [30]:

621 $$c_{post}\frac{dv_{post}}{dt} = c_{cl}\frac{dv_{cl}}{dt} - g_{post}(v_{post} - v_{rest})$$

622 $$2c_{cl}\frac{dv_{cl}}{dt} = c_{cl}\left(\frac{dv_{pre}}{dt} + \frac{dv_{post}}{dt}\right) - g_{cl}v_{cl} + \sum g_{max}p_{open}(v_{pre} - v_{cl} - v_{channel})$$

623 Where g_{max} represents the maximal conductance of a voltage-gated channel, p_{open} the open probability of
624 the voltage-gated channels, which is calculated using a multiple-state model (see below), and $v_{channel}$ the
625 reversal potential of the voltage-gated channel. The reversal potentials were 50 mV, -90 mV, 40 mV and -

70 mV for the sodium conductance, potassium conductance, calcium conductance, and the resting membrane potential of the postsynaptic neuron, respectively. v_{pre} was defined by an AP waveform. Conductance densities in Figure 5 were 0.2 nS μm^{-2} for the sodium conductance, 0.08 nS μm^{-2} for the high-threshold potassium conductance, 0.24 nS μm^{-2} for the low-threshold potassium conductance, and 0.04 nS μm^{-2} for the calcium conductance with a cleft-facing membrane area of 1000 μm^2.

Voltage-gated conductances were modeled with multiple states following ref. [107] except for the calcium conductance. In the models C indicates a closed state, O the open state and I the inactivated state. The sodium channel followed a five states-model, the high-threshold and low-threshold potassium channel were modeled as a six-states channel, and the calcium channel as a two-state channel for which the open probability was squared:

Five states-model: $$C_1 \underset{\beta}{\overset{2\alpha}{\rightleftarrows}} C_2 \underset{2\beta}{\overset{\alpha}{\rightleftarrows}} C_3 \underset{\delta}{\overset{\gamma}{\rightleftarrows}} O \underset{\epsilon}{\overset{\theta}{\rightleftarrows}} I$$

Six states-model: $$C_1 \underset{\beta}{\overset{4\alpha}{\rightleftarrows}} C_2 \underset{2\beta}{\overset{3\alpha}{\rightleftarrows}} C_3 \underset{3\beta}{\overset{2\alpha}{\rightleftarrows}} C_4 \underset{4\beta}{\overset{\alpha}{\rightleftarrows}} C_5 \underset{\delta}{\overset{\gamma}{\rightleftarrows}} O$$

Two states-model: $$C \underset{\beta}{\overset{\alpha}{\rightleftarrows}} O$$

The rate constants indicated by the Greek letters in the state models were calculated as

$$k = a\, e^{b(v_{pre} - v_{cl})}$$

where k represents a particular rate constant, and *a* and *b* are channel-specific parameters listed in Table 1. To take into account a possible effect of the cleft potential on the channel kinetics, the rate constant was calculated using the voltage difference between the presynaptic potential and the cleft potential.

The ordinary differential equations were numerically solved in Igor using IntegrateODE with default settings (fifth-order Runga-Kutta-Fehlberg; step size was adapted to keep $\text{Error}_i < 10^{-6}$; $\text{Error}_i < 10^{-10}$ did not lead to substantial differences in the prespike waveforms).

Statistics are reported as mean and standard deviation. Pearson's correlation coefficient was calculated to quantify correlations. Paired t-tests were performed to compare correlation coefficients from the same data and to compare the absolute deviation from the origin.

Acknowledgements

We thank Dr. Henrique von Gersdorff for helpful discussions on the developmental changes in the prespike.

Table 1. Rate constants for the voltage-gated channels			
		a (ms^{-1})	**b (mV^{-1})**
Sodium conductance	**α**	48.9	1/128.4
	β	1.46	-1/8.9
	γ	392.8	1/36.0
	δ	0.73	-1/15.5
	ε	7.8	1/35.9
	θ	0.01	-1/18
High-threshold potassium conductance	**α**	1.097	1/57.404
	β	0.794	-1/79.264
	γ	33.750	0
	δ	74.360	0
Low-threshold potassium conductance	**α**	1.204	1/37.574
	β	0.360	-1/230
	γ	245.488	0
	δ	132.566	0
Calcium conductance	**α**	1.78	1/23.3
	β	0.14	-1/15
Parameters were taken from ref. [107], except for the calcium conductance [45].			

654

References

1. Foster M. A text-book of physiology: Lea Brothers & Company; 1895.
2. Bennett MR. The early history of the synapse: from Plato to Sherrington. Brain Research Bulletin. 1999;50(2):95-118. doi: 10.1016/S0361-9230(99)00094-5.
3. Sotelo C. The history of the synapse. The Anatomical Record. 2020;303(5):1252-79. doi: 10.1002/ar.24392.
4. Palay SL. Synapses in the central nervous system. The Journal of Cell Biology. 1956;2(4):193-202. doi: 10.1083/jcb.2.4.193.
5. De Robertis E. Submicroscopic changes of the synapse after nerve section in the acoustic ganglion of the guinea pig; an electron microscope study. The Journal of Biophysical and Biochemical Cytology. 1956;2(5):503-12. doi: 10.1083/jcb.2.5.503.
6. Harris KM, Weinberg RJ. Ultrastructure of synapses in the mammalian brain. Cold Spring Harbor perspectives in biology. 2012;4(5):a005587. doi: 10.1101/cshperspect.a005587.
7. Eccles JC, Jaeger JC. The relationship between the mode of operation and the dimensions of the junctional regions at synapses and motor end-organs. Proceedings of the Royal Society of London Series B-Biological Sciences. 1958;148(930):38-56. doi: 10.1098/rspb.1958.0003.
8. Cho S, von Gersdorff H. Proton-mediated block of Ca^{2+} channels during multivesicular release regulates short-term plasticity at an auditory hair cell synapse. The Journal of Neuroscience. 2014;34(48):15877-87. doi: 10.1523/jneurosci.2304-14.2014.
9. DeVries SH. Exocytosed protons feedback to suppress the Ca^{2+} current in mammalian cone photoreceptors. Neuron. 2001;32(6):1107-17. doi: 10.1016/S0896-6273(01)00535-9.
10. Contini D, Price SD, Art JJ. Accumulation of K^+ in the synaptic cleft modulates activity by influencing both vestibular hair cell and calyx afferent in the turtle. The Journal of Physiology. 2017;595(3):777-803. doi: 10.1113/JP273060.
11. Goldberg JM. Theoretical analysis of intercellular communication between the vestibular type I hair cell and its calyx ending. Journal of Neurophysiology. 1996;76(3):1942-57. doi: 10.1152/jn.1996.76.3.1942. PubMed PMID: 8890305.
12. Shih PY, Savtchenko LP, Kamasawa N, Dembitskaya Y, McHugh TJ, Rusakov DA, et al. Retrograde synaptic signaling mediated by K^+ efflux through postsynaptic NMDA receptors. Cell Rep. 2013;5(4):941-51. doi: 10.1016/j.celrep.2013.10.026. PubMed PMID: 24268779.
13. Borst JGG, Sakmann B. Depletion of calcium in the synaptic cleft of a calyx-type synapse in the rat brainstem. Journal of Physiology. 1999;521:123-33. doi: 10.1111/j.1469-7793.1999.00123.x.
14. Stanley EF. Presynaptic calcium channels and the depletion of synaptic cleft calcium ions. J Neurophysiol. 2000;83(1):477-82. doi: 10.1152/jn.2000.83.1.477. PubMed PMID: 10634889.
15. Sylantyev S, Savtchenko LP, Niu Y-P, Ivanov AI, Jensen TP, Kullmann DM, et al. Electric fields due to synaptic currents sharpen excitatory transmission. Science. 2008;319(5871):1845-9. doi: 10.1126/science.1154330.
16. Savtchenko LP, Rusakov DA. The optimal height of the synaptic cleft. Proceedings of the National Academy of Sciences. 2007;104(6):1823. doi: 10.1073/pnas.0606636104.
17. Savtchenko LP, Poo MM, Rusakov DA. Electrodiffusion phenomena in neuroscience: a neglected companion. Nat Rev Neurosci. 2017;18(10):598-612. doi: 10.1038/nrn.2017.101. PubMed PMID: 28924257.
18. Blot A, Barbour B. Ultra-rapid axon-axon ephaptic inhibition of cerebellar Purkinje cells by the pinceau. Nat Neurosci. 2014;17(2):289-95. Epub 2014/01/15. doi: 10.1038/nn.3624. PubMed PMID: 24413696.

19. Rusakov DA, Savtchenko LP, Zheng K, Henley JM. Shaping the synaptic signal: molecular mobility inside and outside the cleft. Trends in Neurosciences. 2011;34(7):359-69. doi: 10.1016/j.tins.2011.03.002.

20. Savtchenko LP, Antropov SN, Korogod SM. Effect of voltage drop within the synaptic cleft on the current and voltage generated at a single synapse. Biophysical Journal. 2000;78(3):1119-25. doi: 10.1016/S0006-3495(00)76670-7.

21. Berretta N, Rossokhin AV, Kasyanov AM, Sokolov MV, Cherubini E, Voronin LL. Postsynaptic hyperpolarization increases the strength of AMPA-mediated synaptic transmission at large synapses between mossy fibers and CA3 pyramidal cells. Neuropharmacology. 2000;39(12):2288-301. doi: 10.1016/s0028-3908(00)00076-9. PubMed PMID: 10974312.

22. Faber DS, Funch PG. Differential properties of orthodromic and antidromic impulse propagation across the Mauthner cell initial segment. Brain Research. 1980;190(1):255-60. doi: 10.1016/0006-8993(80)91176-2.

23. del Castillo J, Katz B. Localization of active spots within the neuromuscular junction of the frog. The Journal of Physiology. 1956;132(3):630-49. doi: 10.1113/jphysiol.1956.sp005554.

24. Martin AR, Pilar G. An analysis of electrical coupling at synapses in the avian ciliary ganglion. J Physiol. 1964;171:454-75. doi: 10.1113/jphysiol.1964.sp007390. PubMed PMID: 14193934; PubMed Central PMCID: PMCPMC1368844.

25. Dmitriev AV, Mangel SC. Electrical feedback in the cone pedicle: A computational analysis. Journal of Neurophysiology. 2006;95(3):1419-27. doi: 10.1152/jn.00098.2005. PubMed PMID: 16319220.

26. Fahrenfort I, Steijaert M, Sjoerdsma T, Vickers E, Ripps H, van Asselt J, et al. Hemichannel-mediated and pH-based feedback from horizontal cells to cones in the vertebrate retina. PLoS One. 2009;4(6):e6090. doi: 10.1371/journal.pone.0006090. PubMed PMID: 19564917; PubMed Central PMCID: PMCPMC2699542.

27. Kamermans M, Fahrenfort I, Schultz K, Janssen-Bienhold U, Sjoerdsma T, Weiler R. Hemichannel-mediated inhibition in the outer retina. Science. 2001;292(5519):1178-80. doi: 10.1126/science.1060101. PubMed PMID: 11349152.

28. Kasyanov AM, Maximov VV, Byzov AL, Berretta N, Sokolov MV, Gasparini S, et al. Differences in amplitude-voltage relations between minimal and composite mossy fibre responses of rat CA3 hippocampal neurons support the existence of intrasynaptic ephaptic feedback in large synapses. Neuroscience. 2000;101(2):323-36. doi: 10.1016/S0306-4522(00)00366-3. PubMed PMID: 11074156.

29. Byzov AL, Shura-Bura TM. Electrical feedback mechanism in the processing of signals in the outer plexiform layer of the retina. Vision Res. 1986;26(1):33-44. doi: 10.1016/0042-6989(86)90069-6. PubMed PMID: 3012877.

30. Savtchenko LP. Bilateral processing in chemical synapses with electrical 'ephaptic' feedback: a theoretical model. Math Biosci. 2007;207(1):113-37. doi: 10.1016/j.mbs.2006.09.016. PubMed PMID: 17112549.

31. Morest DK. The growth of synaptic endings in the mammalian brain: a study of the calyces of the trapezoid body. Zeitschrift für Anatomie und Entwicklungsgeschichte. 1968;127(3):201-20. doi: 10.1007/BF00526129.

32. Rollenhagen A, Lübke JHR. The morphology of excitatory central synapses: from structure to function. Cell Tissue Res. 2006;326(2):221-37. doi: 10.1007/s00441-006-0288-z. PubMed PMID: 16932936.

33. Borst JGG, Soria van Hoeve J. The calyx of Held synapse: from model synapse to auditory relay. Annual Review of Physiology. 2012;74:199-224. Epub 2011/11/01. doi: 10.1146/annurev-physiol-020911-153236. PubMed PMID: 22035348.

34. Forsythe ID. Direct patch recording from identified presynaptic terminals mediating glutamatergic EPSCs in the rat CNS, *in vitro*. J Physiol. 1994;479(3):381-7. doi: 10.1113/jphysiol.1994.sp020303.
35. von Gersdorff H, Borst JGG. Short-term plasticity at the calyx of Held. Nature Reviews Neuroscience. 2002;3:53-64.
36. Borst JGG, Helmchen F, Sakmann B. Pre- and postsynaptic whole-cell recordings in the medial nucleus of the trapezoid body of the rat. J Physiol. 1995;489(Pt 3):825-40. doi: 10.1113/jphysiol.1995.sp021095.
37. Sierksma MC, Slotman JA, Houtsmuller AB, Borst JGG. Structure–function relation of the developing calyx of Held synapse *in vivo*. The Journal of Physiology. 2020;598(20):4603-19. doi: 10.1113/JP279976.
38. Korogod N, Petersen CCH, Knott GW. Ultrastructural analysis of adult mouse neocortex comparing aldehyde perfusion with cryo fixation. Elife. 2015;4. doi: 10.7554/eLife.05793. PubMed PMID: 26259873; PubMed Central PMCID: PMCPMC4530226.
39. Syková E, Nicholson C. Diffusion in brain extracellular space. Physiol Rev. 2008;88(4):1277-340. doi: 10.1152/physrev.00027.2007. PubMed PMID: 18923183.
40. Rubio ME, Nagy JI. Connexin36 expression in major centers of the auditory system in the CNS of mouse and rat: Evidence for neurons forming purely electrical synapses and morphologically mixed synapses. Neuroscience. 2015;303:604-29. Epub 2015/07/19. doi: 10.1016/j.neuroscience.2015.07.026. PubMed PMID: 26188286; PubMed Central PMCID: PMC4576740.
41. Sätzler K, Söhl LF, Bollmann JH, Borst JGG, Frotscher M, Sakmann B, et al. Three-dimensional reconstruction of a calyx of Held and its postsynaptic principal neuron in the medial nucleus of the trapezoid body. J Neurosci. 2002;22(24):10567-79. PubMed PMID: 12486149.
42. Wimmer VC, Horstmann H, Groh A, Kuner T. Donut-like topology of synaptic vesicles with a central cluster of mitochondria wrapped into membrane protrusions: a novel structure-function module of the adult calyx of Held. J Neurosci. 2006;26(1):109-16. doi: 10.1523/JNEUROSCI.3268-05.2006 PubMed PMID: 16399677.
43. Borst JGG, Sakmann B. Calcium influx and transmitter release in a fast CNS synapse. Nature. 1996;383(6599):431-4. doi: 10.1038/383431a0.
44. Borst JGG, Sakmann B. Effect of changes in action potential shape on calcium currents and transmitter release in a calyx-type synapse of the rat auditory brainstem. Philos Trans R Soc Lond B Biol Sci. 1999;354(1381):347-55. doi: 10.1098/rstb.1999.0386. PubMed PMID: 10212483.
45. Borst JGG, Sakmann B. Calcium current during a single action potential in a large presynaptic terminal of the rat brainstem. J Physiol. 1998;506:143-57. doi: 10.1111/j.1469-7793.1998.143bx.x.
46. Wu L-G, Westenbroek RE, Borst JGG, Catterall WE, Sakmann B. Calcium channel types with distinct presynaptic localization couple differentially to transmitter release in single calyx-type synapses. Journal of Neuroscience. 1999;19:726-36. doi: 10.1523/JNEUROSCI.19-02-00726.1999
47. Leão RM, Kushmerick C, Pinaud R, Renden R, Li G-L, Taschenberger H, et al. Presynaptic Na^+ channels: locus, development, and recovery from inactivation at a high-fidelity synapse. J Neurosci. 2005;25(14):3724-38. doi: 10.1523/JNEUROSCI.3983-04.2005. PubMed PMID: 15814803.
48. Berret E, Kim SE, Lee SY, Kushmerick C, Kim JH. Functional and structural properties of ion channels at the nerve terminal depends on compact myelin. J Physiol. 2016;594(19):5593-609. Epub 2016/05/12. doi: 10.1113/JP272205. PubMed PMID: 27168396.
49. Xu J, Berret E, Kim JH. Activity-dependent formation and location of voltage-gated sodium channel clusters at a CNS nerve terminal during postnatal development. Journal of Neurophysiology. 2016. doi: 10.1152/jn.00617.2016.

50. Taschenberger H, von Gersdorff H. Fine-tuning an auditory synapse for speed and fidelity: developmental changes in presynaptic waveform, EPSC kinetics, and synaptic plasticity. J Neurosci. 2000;20(24):9162-73. doi: 10.1523/JNEUROSCI.20-24-09162.2000 PubMed PMID: 11124994.
51. Rowland KC, Irby NK, Spirou GA. Specialized synapse-associated structures within the calyx of Held. J Neurosci. 2000;20(24):9135-44. doi: 10.1523/JNEUROSCI.20-24-09135.2000. PubMed PMID: 11124991.
52. Ford MC, Grothe B, Klug A. Fenestration of the calyx of Held occurs sequentially along the tonotopic axis, is influenced by afferent activity, and facilitates glutamate clearance. J Comp Neurol. 2009;514(1):92-106. PubMed PMID: 19260071.
53. Kandler K, Friauf E. Pre- and postnatal development of efferent connections of the cochlear nucleus in the rat. Journal of Comparative Neurology. 1993;328(2):161-84. doi: 10.1002/cne.903280202.
54. Ryugo DK, Montey KL, Wright AL, Bennett ML, Pongstaporn T. Postnatal development of a large auditory nerve terminal: the endbulb of Held in cats. Hear Res. 2006;216-217:100-15. Epub 2006/02/25. doi: 10.1016/j.heares.2006.01.007. PubMed PMID: 16497457.
55. Hess A, Pilar G, Weakly JN. Correlation between transmission and structure in avian ciliary ganglion synapses. J Physiol. 1969;202(2):339-54. doi: 10.1113/jphysiol.1969.sp008815. PubMed PMID: 4306543; PubMed Central PMCID: PMCPMC1351486.
56. Baydyuk M, Xu J, Wu LG. The calyx of Held in the auditory system: Structure, function, and development. Hear Res. 2016;338:22-31. Epub 2016/03/29. doi: 10.1016/j.heares.2016.03.009. PubMed PMID: 27018297; PubMed Central PMCID: PMC4967386.
57. Spirou GA, Chirila FV, von Gersdorff H, Manis PB. Heterogeneous Ca^{2+} influx along the adult calyx of Held: a structural and computational study. Neuroscience. 2008;154(1):171-85. PubMed PMID: 18485608.
58. Wang T, van Woerden GM, Elgersma Y, Borst JGG. Enhanced transmission at the calyx of Held synapse in a mouse model for Angelman syndrome. Front Cell Neurosci. 2017;11:418. Epub 2018/01/23. doi: 10.3389/fncel.2017.00418. PubMed PMID: 29354033; PubMed Central PMCID: PMC5758499.
59. Lorteije JAM, Rusu SI, Kushmerick C, Borst JGG. Reliability and precision of the mouse calyx of Held synapse. J Neurosci. 2009;29(44):13770-84. doi: 10.1523/JNEUROSCI.3285-09.2009. PubMed PMID: 19889989.
60. Barnes-Davies M, Forsythe ID. Pre- and postsynaptic glutamate receptors at a giant excitatory synapse in rat auditory brainstem slices. Journal of Physiology. 1995;488(2):387-406. doi: 10.1113/jphysiol.1995.sp020974.
61. Forsythe ID, Barnes-Davies M. The binaural auditory pathway: excitatory amino acid receptors mediate dual timecourse excitatory postsynaptic currents in the rat medial nucleus of the trapezoid body. Proceedings of the Royal Society B. 1993;251(1331):151-7. doi: 10.1098/rspb.1993.0022.
62. Joshi I, Wang L-Y. Developmental profiles of glutamate receptors and synaptic transmission at a single synapse in the mouse auditory brainstem. J Physiol. 2002;540(Pt 3):861-73. doi: 10.1113/jphysiol.2001.013506. PubMed PMID: 11986375.
63. Yang Y-M, Wang L-Y. Amplitude and kinetics of action potential-evoked Ca^{2+} current and its efficacy in triggering transmitter release at the developing calyx of Held synapse. J Neurosci. 2006;26(21):5698-708. doi: 10.1523/JNEUROSCI.4889-05.2006 PubMed PMID: 16723526.
64. Fekete A, Nakamura Y, Yang YM, Herlitze S, Mark MD, DiGregorio DA, et al. Underpinning heterogeneity in synaptic transmission by presynaptic ensembles of distinct morphological modules. Nat Commun. 2019;10(1):826. Epub 2019/02/20. doi: 10.1038/s41467-019-08452-2. PubMed PMID: 30778063; PubMed Central PMCID: PMC6379440.
65. Martin AR, Pilar G. Transmission through the ciliary ganglion of the chick. Journal of Physiology. 1963;168:464-75.

66. Funch PG, Faber DS. Action-potential propagation and orthodromic impulse initiation in Mauthner axon. Journal of Neurophysiology. 1982;47(6):1214-31. doi: 10.1152/jn.1982.47.6.1214
67. Vandenbranden CA, Verweij J, Kamermans M, Muller LJ, Ruijter JM, Vrensen GF, et al. Clearance of neurotransmitter from the cone synaptic cleft in goldfish retina. Vision Research. 1996;36(24):3859-74. doi: 10.1016/s0042-6989(96)00134-4.
68. DeVries SH, Li W, Saszik S. Parallel processing in two transmitter microenvironments at the cone photoreceptor synapse. Neuron. 2006;50(5):735-48. doi: 10.1016/j.neuron.2006.04.034. PubMed PMID: 16731512.
69. Baumann SB, Wozny DR, Kelly SK, Meno FM. The electrical conductivity of human cerebrospinal fluid at body temperature. IEEE Trans Biomed Eng. 1997;44(3):220-3. doi: 10.1109/10.554770. PubMed PMID: 9216137.
70. Roth A, Häusser M. Compartmental models of rat cerebellar Purkinje cells based on simultaneous somatic and dendritic patch-clamp recordings. J Physiol. 2001;535(Pt 2):445-72. doi: 10.1111/j.1469-7793.2001.00445.x. PubMed PMID: 11533136.
71. Golding NL, Mickus TJ, Katz Y, Kath WL, Spruston N. Factors mediating powerful voltage attenuation along CA1 pyramidal neuron dendrites. J Physiol. 2005;568(Pt 1):69-82. doi: 10.1113/jphysiol.2005.086793. PubMed PMID: 16002454; PubMed Central PMCID: PMCPMC1474764.
72. Cohen CCH, Popovic MA, Klooster J, Weil MT, Mobius W, Nave KA, et al. Saltatory conduction along myelinated axons involves a periaxonal nanocircuit. Cell. 2020;180(2):311-22 e15. doi: 10.1016/j.cell.2019.11.039. PubMed PMID: 31883793; PubMed Central PMCID: PMCPMC6978798.
73. Zheng K, Jensen TP, Savtchenko LP, Levitt JA, Suhling K, Rusakov DA. Nanoscale diffusion in the synaptic cleft and beyond measured with time-resolved fluorescence anisotropy imaging. Scientific Reports. 2017;7(1):42022. doi: 10.1038/srep42022.
74. Land BR, Harris WV, Salpeter EE, Salpeter MM. Diffusion and binding constants for acetylcholine derived from the falling phase of miniature endplate currents. Proc Natl Acad Sci U S A. 1984;81(5):1594-8. doi: 10.1073/pnas.81.5.1594. PubMed PMID: 6584895; PubMed Central PMCID: PMCPMC344884.
75. Faber DS, Funch PG, Korn H. Evidence that receptors mediating central synaptic potentials extend beyond the postsynaptic density. Proc Natl Acad Sci U S A. 1985;82(10):3504-8. doi: 10.1073/pnas.82.10.3504. PubMed PMID: 2582417; PubMed Central PMCID: PMCPMC397805.
76. Nielsen TA, DiGregorio DA, Silver RA. Modulation of glutamate mobility reveals the mechanism underlying slow-rising AMPAR EPSCs and the diffusion coefficient in the synaptic cleft. Neuron. 2004;42(5):757-71. doi: 10.1016/j.neuron.2004.04.003. PubMed PMID: 15182716.
77. Guinan JJ, Jr., Li RY-S. Signal processing in brainstem auditory neurons which receive giant endings (calyces of Held) in the medial nucleus of the trapezoid body of the cat. Hear Res. 1990;49(1-3):321-34. doi: 10.1016/0378-5955(90)90111-2.
78. Pfeiffer RR. Anteroventral cochlear nucleus: wave forms of extracellularly recorded spike potentials. Science. 1966;154(749):667-8. doi: 10.1126/science.154.3749.667 PubMed PMID: 5923782.
79. Typlt M, Haustein MD, Dietz B, Steinert JR, Witte M, Englitz B, et al. Presynaptic and postsynaptic origin of multicomponent extracellular waveforms at the endbulb of Held-spherical bushy cell synapse. Eur J Neurosci. 2010;31(9):1574-81. Epub 2010/06/09. doi: 10.1111/j.1460-9568.2010.07188.x. PubMed PMID: 20525070.
80. Eysel UT. Quantitative studies of intracellular postsynaptic potentials in the lateral geniculate nucleus of the cat with respect to optic tract stimulus response latencies. Exp Brain Res. 1976;25:469-86. doi: 10.1007/bf00239782. PubMed PMID: 182514.
81. Dudel J. Effect of inhibition on the presynaptic nerve terminal in the neuromuscular junction of the crayfish. Nature. 1962;193:587-8. doi: 10.1038/193587b0. PubMed PMID: 13888196.

885 82. Takeuchi A, Takeuchi N. Electrical changes in pre- and postsynaptic axons of the giant synapse of
886 Loligo. J Gen Physiol. 1962;45:1181-93. doi: 10.1085/jgp.45.6.1181. PubMed PMID: 13919241; PubMed
887 Central PMCID: PMCPMC2195243.
888 83. Katz B, Miledi R. Propagation of electric activity in motor nerve terminals. Proceedings of the
889 Royal Society B. 1965;161:453-82. doi: 10.1098/rspb.1965.0015.
890 84. Mathy A, Ho SSN, Davie JT, Duguid IC, Clark BA, Häusser M. Encoding of oscillations by axonal
891 bursts in inferior olive neurons. Neuron. 2009;62(3):388-99. Epub 2009/05/19. doi:
892 10.1016/j.neuron.2009.03.023. PubMed PMID: 19447094; PubMed Central PMCID: PMC2777250.
893 85. Maruta J, Hensbroek RA, Simpson JI. Intraburst and interburst signaling by climbing fibers. J
894 Neurosci. 2007;27(42):11263-70. Epub 2007/10/19. doi: 10.1523/JNEUROSCI.2559-07.2007. PubMed
895 PMID: 17942720.
896 86. Michalikova M, Remme MWH, Schmitz D, Schreiber S, Kempter R. Spikelets in pyramidal
897 neurons: generating mechanisms, distinguishing properties, and functional implications. Rev Neurosci.
898 2019;31(1):101-19. doi: 10.1515/revneuro-2019-0044. PubMed PMID: 31437125.
899 87. Vigmond EJ, Perez Velazquez JL, Valiante TA, Bardakjian BL, Carlen PL. Mechanisms of electrical
900 coupling between pyramidal cells. J Neurophysiol. 1997;78(6):3107-16. doi: 10.1152/jn.1997.78.6.3107.
901 PubMed PMID: 9405530.
902 88. Sierksma MC, Tedja MS, Borst JGG. *In vivo* matching of postsynaptic excitability with
903 spontaneous synaptic inputs during formation of the rat calyx of Held synapse. J Physiol.
904 2016;595(1):207-31. Epub 2016/07/19. doi: 10.1113/JP272780. PubMed PMID: 27426483.
905 89. Holcomb PS, Hoffpauir BK, Hoyson MC, Jackson DR, Deerinck TJ, Marrs GS, et al. Synaptic inputs
906 compete during rapid formation of the calyx of Held: a new model system for neural development. J
907 Neurosci. 2013;33(32):12954-69. Epub 2013/08/09. doi: 10.1523/JNEUROSCI.1087-13.2013. PubMed
908 PMID: 23926251; PubMed Central PMCID: PMC3735879.
909 90. Ritzau-Jost A, Delvendahl I, Rings A, Byczkowicz N, Harada H, Shigemoto R, et al. Ultrafast action
910 potentials mediate kilohertz signaling at a central synapse. Neuron. 2014;84(1):152-63. doi:
911 10.1016/j.neuron.2014.08.036.
912 91. Sierksma MC, Borst JGG. Resistance to action potential depression of a rat axon terminal in vivo.
913 Proc Natl Acad Sci U S A. 2017;114(16):4249-54. Epub 2017/04/05. doi: 10.1073/pnas.1619433114.
914 PubMed PMID: 28373550; PubMed Central PMCID: PMC5402426.
915 92. Lin KH, Oleskevich S, Taschenberger H. Presynaptic Ca^{2+} influx and vesicle exocytosis at the
916 mouse endbulb of Held: a comparison of two auditory nerve terminals. J Physiol. 2011;589(17):4301-20.
917 doi: 10.1113/jphysiol.2011.209189. PubMed PMID: 21746778; PubMed Central PMCID:
918 PMCPMC3180584.
919 93. Rancz EA, Ishikawa T, Duguid I, Chadderton P, Mahon S, Häusser M. High-fidelity transmission of
920 sensory information by single cerebellar mossy fibre boutons. Nature. 2007;450(7173):1245-8. doi:
921 10.1038/nature05995. PubMed PMID: 18097412.
922 94. Geiger JR, Jonas P. Dynamic control of presynaptic Ca^{2+} inflow by fast-inactivating K^+ channels in
923 hippocampal mossy fiber boutons. Neuron. 2000;28(3):927-39. PubMed PMID: 11163277.
924 95. Bischofberger J, Geiger JRP, Jonas P. Timing and efficacy of Ca^{2+} channel activation in
925 hippocampal mossy fiber boutons. J Neurosci. 2002;22(24):10593-602. Epub 2002/12/18. doi:
926 10.1523/JNEUROSCI.22-24-10593.2002 PubMed PMID: 12486151.
927 96. Ritzau-Jost A, Tsintsadze T, Krueger M, Ader J, Bechmann I, Eilers J, et al. Large, stable spikes
928 exhibit differential broadening in excitatory and inhibitory neocortical boutons. Cell Rep.
929 2021;34(2):108612. doi: 10.1016/j.celrep.2020.108612. PubMed PMID: 33440142; PubMed Central
930 PMCID: PMCPMC7809622.
931 97. Furukawa T, Furshpan EJ. Two inhibitory mechanisms in the Mauthner neurons of goldfish. J
932 Neurophysiol. 1963;26:140-76. doi: 10.1152/jn.1963.26.1.140. PubMed PMID: 13945908.

98. Tatsuoka H, Reese TS. New structural features of synapses in the anteroventral cochlear nucleus prepared by direct freezing and freeze-substitution. Journal of Comparative Neurology. 1989;290(3):343-57. doi: 10.1002/cne.902900304.
99. Nakajima Y. Fine structure of the medial nucleus of the trapezoid body of the bat with special reference to two types of synaptic endings. J Cell Biol. 1971;50(1):121-34. doi: 10.1083/jcb.50.1.121
100. Blosa M, Sonntag M, Jäger C, Weigel S, Seeger J, Frischknecht R, et al. The extracellular matrix molecule brevican is an integral component of the machinery mediating fast synaptic transmission at the calyx of Held. J Physiol. 2015;593(19):4341-60. Epub 2015/08/01. doi: 10.1113/jp270849. PubMed PMID: 26223835.
101. Martin R, Miledi R. The form and dimensions of the giant synapse of squids. Philosophical Transactions of the Royal Society B. 1986;312(1155):355-77. doi: 10.1098/rstb.1986.0013.
102. Sanes JR, Lichtman JW. Development of the vertebrate neuromuscular junction. Annu Rev Neurosci. 1999;22:389-442. Epub 1999/04/15. doi: 10.1146/annurev.neuro.22.1.389. PubMed PMID: 10202544.
103. Renden R, Taschenberger H, Puente N, Rusakov DA, Duvoisin R, Wang L-Y, et al. Glutamate transporter studies reveal the pruning of metabotropic glutamate receptors and absence of AMPA receptor desensitization at mature calyx of Held synapses. J Neurosci. 2005;25(37):8482-97. doi: 10.1523/JNEUROSCI.1848-05.2005. PubMed PMID: 16162930.
104. Taschenberger H, Leão RM, Rowland KC, Spirou GA, von Gersdorff H. Optimizing synaptic architecture and efficiency for high-frequency transmission. Neuron. 2002;36(6):1127-43. doi: 10.1016/S0896-6273(02)01137-6. PubMed PMID: 12495627.
105. Graydon CW, Cho S, Diamond JS, Kachar B, von Gersdorff H, Grimes WN. Specialized postsynaptic morphology enhances neurotransmitter dilution and high-frequency signaling at an auditory synapse. J Neurosci. 2014;34(24):8358-72. doi: 10.1523/JNEUROSCI.4493-13.2014. PubMed PMID: 24920639; PubMed Central PMCID: PMCPMC4051984.
106. Cathala L, Holderith NB, Nusser Z, DiGregorio DA, Cull-Candy SG. Changes in synaptic structure underlie the developmental speeding of AMPA receptor-mediated EPSCs. Nat Neurosci. 2005;8(10):1310-8. doi: 10.1038/nn1534. PubMed PMID: 16172604.
107. Yang YM, Wang W, Fedchyshyn MJ, Zhou Z, Ding J, Wang LY. Enhancing the fidelity of neurotransmission by activity-dependent facilitation of presynaptic potassium currents. Nat Commun. 2014;5:4564. Epub 2014/08/01. doi: 10.1038/ncomms5564. PubMed PMID: 25078759.
108. Borst JGG, Helmchen F. Calcium influx during an action potential. In: Conn PM, editor. Methods in Enzymology. Ion Channels. 293: Academic Press; 1998. p. 352-71.

Appendix A1. Analysis of the electronic model

Following Kirchhoff's current law, the sum of the currents that enter the cleft must be equal to the sum of the currents leaving the cleft:

$i_{leave} = i_{enter}$ $(A1.1)$.

The currents that enter the cleft are either resistive or capacitive, coming either from the presynaptic or the postsynaptic side; we also included the conductances of presynaptic voltage-gated channels (g_{ion}) (Figure 2B):

$$i_{enter} = g_{pre}(v_{pre} - v_{pre,rest}) + c_{pre}\frac{dv_{pre}}{dt} + g_{syn}(v_{post} - v_{post,rest}) + c_{syn}\frac{dv_{post}}{dt} + \sum g_{ion}(v_{pre} - v_{ion}) \qquad (A1.2)$$

where v_{pre} and v_{post} are the pre- and the postsynaptic membrane potential relative to the interstitial fluid, respectively, $v_{pre,rest}$ and $v_{post,rest}$ are the pre- and the postsynaptic resting membrane potential relative to the interstitial fluid, respectively, c_{pre} and c_{syn} are the capacitances of the pre- and the postsynaptic membrane facing the cleft, respectively, and g_{pre} and g_{syn} and the resting, leak conductance of the pre- and postsynaptic membrane facing the cleft, respectively (Figure 2). The summation sign indicates the summation of the different types of voltage-gated channels, each with their own time- and voltage-dependent conductance g_{ion} and their own reversal potential v_{ion} relative to the extracellular fluid.

The currents leaving the cleft are resistive through a cleft leak conductance (g_{cl}), and resistive and capacitive through the presynaptic and postsynaptic side:

$$i_{leave} = v_{cl}\left(g_{cl} + g_{pre} + g_{syn} + \sum g_{ion}\right) + (c_{pre} + c_{syn})\frac{dv_{cl}}{dt} \qquad (A1.3)$$

This gives the full equation for the cleft (combine Eqs. A1.1-3), similar to ref. [30]:

$$v_{cl}\left(g_{cl}+g_{syn}+g_{pre}+\sum g_{ion}\right)+\left(c_{pre}+c_{syn}\right)\frac{dv_{cl}}{dt}$$

$$= g_{pre}\left(v_{pre}-v_{pre,rest}\right)+c_{pre}\frac{dv_{pre}}{dt}+g_{syn}\left(v_{post}-v_{post,rest}\right)+c_{syn}\frac{dv_{post}}{dt}$$

$$+\sum g_{ion}(v_{pre}-v_{ion}) \quad (A1.4)$$

We simplify the full equation by assuming that the postsynaptic currents entering the cleft (g_{syn} (v_{post} - $v_{post,rest}$) + $c_{syn}dv_{post}/dt$) are much smaller than the presynaptic currents entering the cleft, as is the case when the prespike is very small, and therefore can be neglected. For the calyx of Held synapse, the postsynaptic, cleft-facing, resting conductance is indeed rather small (g_{syn} < 3 nS, excluding the conductance of the EPSC), and the prespike is at most a few mV. The presynaptic capacitive currents during the presynaptic AP are much larger than the resistive currents, as g_{pre} < 5 nS, generating currents less than 0.6 nA (<120 mV x 5 nS), while the presynaptic capacitive current can easily be 5 nA (500 V/s x 10 pF). We thus derive the following, simplified equation:

$$v_{cl}\left(g_{cl}+\sum g_{ion}\right)+\left(c_{pre}+c_{syn}\right)\frac{dv_{cl}}{dt}=c_{pre}\frac{dv_{pre}}{dt}+\sum g_{ion}\left(v_{pre}-v_{ion}\right) \quad (A1.5)$$

For a given synapse, we can distinguish two extreme scenarios depending on the route currents entering the cleft may take: resistive versus capacitive dissipation. If the cleft currents mainly dissipate via capacitive routes (membrane, $v_{cl}(g_{cl} + \Sigma g_{ion}) << (c_{pre} + c_{syn})dv_{cl}/dt$). Eq. A1.5 can be simplified to:

$$\left(c_{pre}+c_{syn}\right)\frac{dv_{cl}}{dt}=c_{pre}\frac{dv_{pre}}{dt}+\sum g_{ion}\left(v_{pre}-v_{ion}\right) \quad (A1.6)$$

$$\frac{dv_{cl}}{dt}=\frac{c_{pre}}{c_{pre}+c_{syn}}\frac{dv_{pre}}{dt}+\frac{1}{c_{pre}+c_{syn}}\sum g_{ion}\left(v_{pre}-v_{ion}\right) \quad (A1.7)$$

$$v_{cl} = \int \left(\frac{c_{pre}}{c_{pre} + c_{syn}} \frac{dv_{pre}}{dt} + \frac{1}{c_{pre} + c_{syn}} \sum g_{ion} \left(v_{pre} - v_{ion} \right) \right) dt$$

$$= \frac{c_{pre}}{c_{pre} + c_{syn}} v_{pre} + \frac{1}{c_{pre} + c_{syn}} \int \left(\sum g_{ion} \left(v_{pre} - v_{ion} \right) \right) dt + v_{constant} \qquad (A1.8)$$

The VC prespike becomes (using eq. A1.7):

$$-i_{rec} = c_{syn} \frac{dv_{cl}}{dt} = \frac{c_{syn}}{c_{pre} + c_{syn}} \left(c_{pre} \frac{dv_{pre}}{dt} + \sum g_{ion} \left(v_{pre} - v_{ion} \right) \right) \qquad (A1.9)$$

Note that in the capacitive dissipation scenario, cleft currents dissipate as a postsynaptic as well as a presynaptic capacitive current. The relative fraction that dissipates through the presynaptic and postsynaptic membrane equals c_{pre} $(c_{pre}+c_{syn})^{-1}$ and c_{syn} $(c_{pre}+c_{syn})^{-1}$, respectively. In other words, the presynaptic currents are partially reflected back to the presynaptic side in this scenario. For the calyx of Held synapse, where the presynaptic and postsynaptic capacitance are nearly equal, the relative fraction equals 0.5.

In the resistive dissipation scenario we consider the case where the cleft currents mainly dissipate via resistive routes ($v_{cl}(g_{cl} + \Sigma g_{ion}) >> (c_{pre} + c_{syn}) dv_{cl}/dt$).We can neglect the contribution of the capacitive currents induced by the cleft potential to derive the equation for the cleft potential. Eq. A1.5 can then be simplified to:

$$v_{cl} \left(g_{cl} + \sum g_{ion} \right) = c_{pre} \frac{dv_{pre}}{dt} + \sum g_{ion} \left(v_{pre} - v_{ion} \right) \qquad (A1.10)$$

$$v_{cl} = \left(g_{cl} + \sum g_{ion} \right)^{-1} \left(c_{pre} \frac{dv_{pre}}{dt} + \sum g_{ion} \left(v_{pre} - v_{ion} \right) \right) \qquad (A1.11)$$

An additional simplification is justified if $g_{cl} >> \Sigma g_{ion}$:

$$v_{cl} = (g_{cl})^{-1}\left(c_{pre}\frac{dv_{pre}}{dt} + \sum g_{ion}\left(v_{pre} - v_{ion}\right)\right) \qquad (A1.12)$$

In this case, v_{cl} becomes a scaled sum of the first derivative of the presynaptic AP and ionic currents through voltage-gated channels.

The postsynaptic prespike, when recorded in voltage-clamp, still equals the capacitive current over the postsynaptic membrane, which now is assumed to be much smaller than the currents that are present in the cleft:

$$-i_{rec} = c_{syn}\frac{dv_{cl}}{dt} = c_{syn}\frac{d}{dt}\left((g_{cl})^{-1}\left(c_{pre}\frac{dv_{pre}}{dt} + \sum g_{ion}\left(v_{pre} - v_{ion}\right)\right)\right)$$

$$= \frac{c_{syn}c_{pre}}{g_{cl}}\frac{d^2v_{pre}}{dt^2} + \frac{c_{syn}}{g_{cl}}\sum\frac{d}{dt}\left(g_{ion}\left(v_{pre} - v_{ion}\right)\right) \qquad (A1.13)$$

For the CC prespike, in both situations, the current entering the postsynaptic cell via the cleft membrane must be equal to the current leaving the cell:

$$c_{post}\frac{dv_{post}}{dt} + g_{post}\left(v_{post} - v_{post,rest}\right) = -i_{rec} = c_{syn}\frac{dv_{cl}}{dt} + g_{syn}v_{cl} \qquad (A1.14)$$

Where c_{post} and g_{post} are the total postsynaptic capacitance and conductance, respectively (Figure 2). The shape of the CC prespike will depend on the cleft potential, the cleft-facing capacitance and the conductance of the cleft-facing membrane, allowing a large range of different prespike shapes (reflecting the integral of the cleft potential, the cleft potential itself, or the first derivative of the cleft potential).

We can simplify the notation of some equations by defining a cleft time constant ($\tau_{cl} = c_{cl}/g_{cl}$), and and $c_{cl} = c_{syn} = c_{pre}$. The equations then become remarkably simple:

$$v_{cl} = \frac{1}{g_{cl}}\left(c_{cl}\frac{dv_{pre}}{dt} + \sum g_{ion}\left(v_{pre} - v_{ion}\right)\right) = \frac{i_{cleft}}{g_{cl}} \qquad (A1.15)$$

$$-i_{rec} = c_{cl}\frac{dv_{cl}}{dt} = \tau_{cl}\frac{di_{cleft}}{dt} \qquad (A1.16)$$

$$c_{post}\frac{dv_{post}}{dt} + g_{post}v_{post} = -i_{rec} = \tau_{cl}\frac{di_{cleft}}{dt} = c_{cl}\frac{dv_{cl}}{dt} \qquad (A1.17)$$

If we furthermore assume that $g_{post}(v_{post} - v_{post,rest}) << c_{post}\, dv_{post}/dt$:

$$c_{post}\frac{dv_{post}}{dt} = \tau_{cl}\frac{di_{enter}}{dt} = c_{cl}\frac{dv_{cl}}{dt}$$

$$v_{post} = \frac{c_{cl}}{c_{post}g_{cl}}i_{enter} + v_{post,rest} = \frac{c_{cl}}{c_{post}}v_{cl} + v_{post,rest} \qquad (A1.18)$$

The cleft potential is then defined by Ohm's law: the ratio of the net current that runs through the cleft and the cleft leak conductance. The VC prespike is defined by the first derivative of the net currents scaled by the cleft time constant. The CC prespike is defined by the cleft potential and the fraction of the postsynaptic capacitance facing the cleft.

Appendix A2. The calcium prespike

This Appendix deals with the question how the recorded calcium current contributes to the VC prespike. The current i_{ion} that runs through the presynaptic cleft-facing membrane can leak away either capacitively or resistively similar to the capacitive currents from the presynaptic AP. The recorded calcium current typically closely follows a Gaussian function [45, 108]:

$$i_{ca} = i_{max}e^{t^2/(-2\tau_{Ca}{}^2)} \qquad (A2.1)$$

For the capacitive dissipation scenario, we rewrite A1.9:

$$-i_{rec} = c_{syn}\frac{dv_{cl}}{dt} = c_{pre}\frac{d(v_{pre} - v_{cl})}{dt} + i_{Ca} \qquad (A2.2)$$

When we subtract the passive prespike ($i_{\text{passive-cap}}$) from the prespike recording, we arrive at the calcium prespike:

$$-i_{rec} + i_{passive-cap} = i_{ca} \qquad (A2.3)$$

For the resistive dissipation scenario, we rewrite A1.19 and we again subtract the passive prespike ($i_{\text{passive-res}}$) to arrive at the calcium prespike:

$$-i_{rec} + i_{passive-res} = \tau_{cl}\frac{di_{ca}}{dt} = \tau_{cl} i_{max}\frac{d}{dt}\left(e^{t^2/(-2\tau_{Ca}{}^2)}\right) = \frac{\tau_{cl} i_{max}}{\tau_{Ca}{}^2}\, t\, e^{t^2/(-2\tau_{Ca}{}^2)} \qquad (A2.4)$$

This equation shows two peaks at $t = \pm\tau_{Ca}$ with an amplitude of

$$-i_{rec}(\tau_{Ca}) + i_{passive-res}(\tau_{Ca}) = \pm\frac{\tau_{cl} i_{max}}{\tau_{Ca}{}^2}\,\tau_{Ca}\, e^{(\pm\tau_{Ca})^2/(-2\tau_{Ca}{}^2)} = \pm\frac{\tau_{cl}}{\tau_{Ca}\sqrt{e}} i_{max} \qquad (A2.5)$$

We thus define a simple scaling factor $\tau_{cl}(\tau_{Ca}\sqrt{e})^{-1}$ that relates the amplitude of the presynaptic calcium current to the amplitude of the calcium prespike.

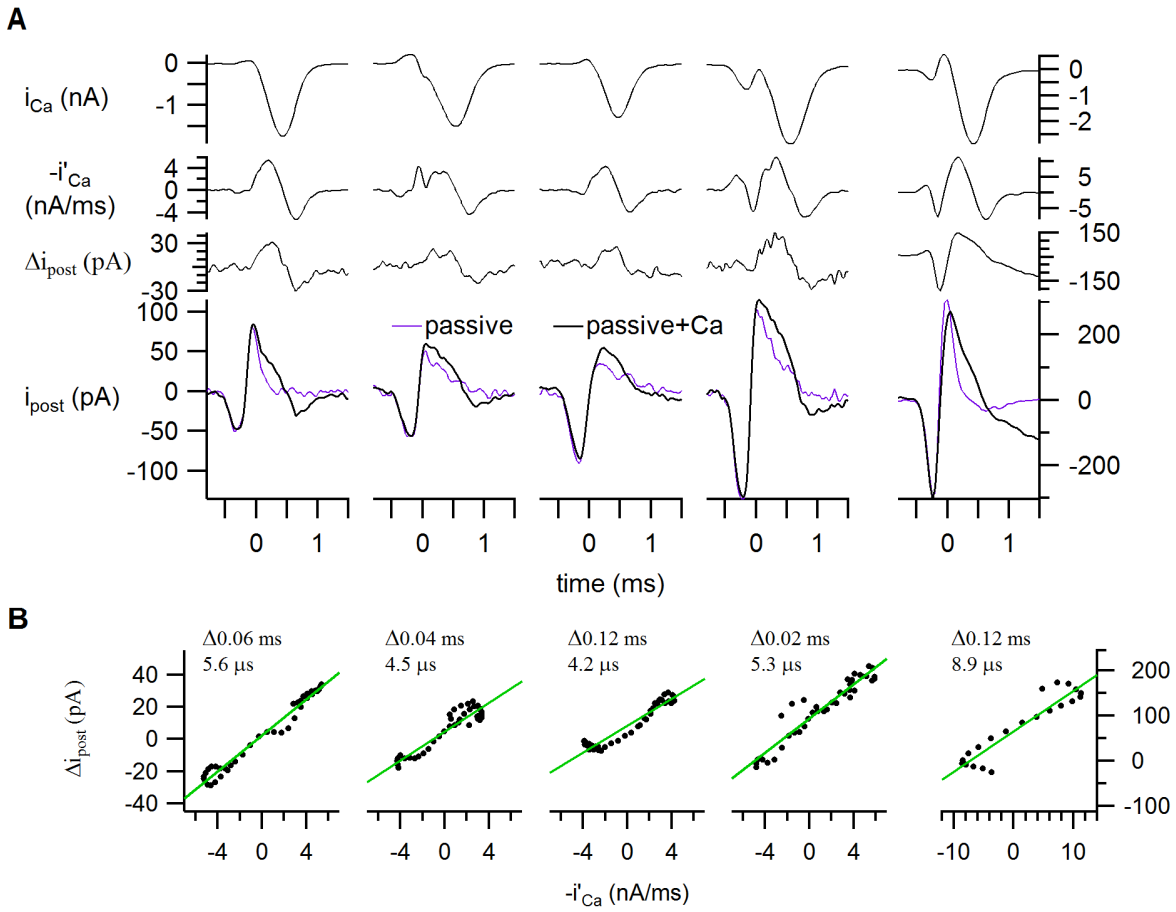

Figure S1 – Relation between the calcium current and the prespike, continued. Our data set was composed of five double recordings. The presynaptic voltage-clamp waveform is shown in Figure 4A. (A) *from top to bottom*: The presynaptic calcium current (after P/5 subtraction), its inverted first derivative, the calcium prespike, and the active (black, thick) and passive prespike (magenta, P/5-scaled). Voltage-gated sodium and potassium currents were blocked (see methods). The left-most column is also shown in Figure 4A. The right-most is the only one plotted on scaling of the axes on the right. Notice how even when the presynaptic calcium current does not smoothly follow a Gaussian function, its first derivative resembles the calcium prespike as predicted from our analytical relations for the resistive dissipation scenario. (B) Relation between the inverted first derivative of the presynaptic calcium current and the calcium prespike (black dots). Maximum correlation was obtained by introducing a delay for the first derivative. This delay and the slope of the regression line are shown in the top left corner of each panel. Each panel corresponds the example in the same column in A.

Appendix B. Geometry

Question B1: What is the voltage profile in the synaptic cleft for a simplified synapse?

We assume a radially-symmetrical synapse with radius *r* and cleft height *h*. The capacitive current that enters the synaptic cleft equals:

$$i_{cap} = c_m v'_{pre} = C_m \pi r^2 v'_{pre} \qquad \text{(B1.1)}$$

with v'_{pre} indicating the first temporal derivative of the presynaptic AP. We assume that the current is homogeneously distributed over the cleft-facing membrane and that all currents within the cleft run radially towards the interstitial fluid (resistive dissipation). The current density $J(x)$ can be defined as a quasi-static function of the radial location *x,* where 0 indicates the center and *r* the synapse edge. J(x) will be equal to the current that runs through the cleft-facing membrane from the center to radius x divided by the surface through which it escapes, $A_{esc}(x)$. This surface is the surface of an open cylinder with radius x and height *h*:

$$J(x) = \frac{i(x)}{A_{esc}(x)} = \frac{\pi x^2 C_m v'_{pre}}{2\pi x h} = \frac{C_m v'_{pre}}{2h} x \qquad \text{(B1.2)}$$

Based on $J(x)$, the electric field can be defined using a homogeneous extracellular cleft resistivity R_{ex}, where the negative sign reflects the convention that current runs down the voltage gradient:

$$-\frac{dv(x)}{dx} = R_{ex} J(x) = \frac{R_{ex} C_m v'_{pre}}{2h} x \qquad \text{(B1.3)}$$

The voltage profile relative to the cleft edge is the integral of equation B1.3 from x to r:

$$v(x) = \int_x^r \left(-\frac{R_{ex} C_m v'_{pre}}{2h} x\right) dx = -\frac{R_{ex} C_m v'_{pre}}{2h} \int_x^r (x) dx = \frac{R_{ex} C_m v'_{pre}}{4h} (r^2 - x^2) \qquad \text{(B1.4)}$$

We can also rewrite equation B1.4 as a relative distance to the cleft edge:

$$v(x/r) = \frac{r^2 R_{ex} C_m v'_{pre}}{4h}(1-(x/r)^2) \qquad \text{(B1.5)}$$

The voltage profile will apply as long as all current runs radially to the extracellular matrix. When this is not the case -for instance, when currents enter into the postsynaptic cell or return through the presynaptic cleft-facing membrane- the current density will be reduced, and the voltage gradient will be reduced as well.

Question B2: How much current will be generated at the postsynaptic membrane?

We assume that the currents that run through the postsynaptic membrane are purely capacitive:

$$i_{post} = \int_{x=0}^{r} i_{cap}(x)dx = \int_{x=0}^{r} (C_m A(x) v'(x))dx \qquad \text{(B2.1)}$$

Here, the current through an annulus of membrane (at x, with thickness dx) will depend on the radial location as the surface of the annulus equals $2\pi x dx$ and the cleft potential is also defined by the radial location (equation B1.4). Only v'_{pre} will be affected by the time derivative, which will become the second time derivative (v''_{pre}) . The equation then becomes:

$$i_{post} = C_m \int_{x=0}^{r} \left(2\pi x \, \frac{R_{ex} C_m v''_{pre}}{4h} \, (r^2 - x^2)\right) dx$$

$$= \frac{\pi R_{ex} C_m^2 v''_{pre}}{2h} \int_{x=0}^{r} (x\,(r^2 - x^2))dx$$

$$= \frac{\pi R_{ex} C_m^2 v''_{pre}}{2h} \left[\frac{1}{2} r^2 x^2 - \frac{1}{4} x^4\right]_{x=0}^{r}$$

$$= \frac{\pi R_{ex} C_m^2 v''_{pre}}{8h} r^4 \qquad \text{(B2.2)}$$

Question B3: How does the cleft resistivity relate to the cleft conductance?

We noted that B2.2 resembles A1.19 without the voltage-gated currents: :

$$i_{post} = \frac{{c_{cl}}^2}{g_{cl}} v''_{pre} = \frac{(C_m \pi r^2)^2}{g_{cl}} v''_{pre} \qquad \text{(B3.1)}$$

By combining equation B2.2 and B3.1 we find that g_{cl} relates to the cleft resistivity:

$$g_{cl} = \frac{8\pi h}{R_{ex}} \qquad \text{(B3.2)}$$

Combining equations B3.1 and B3.2 yields an alternative way to calculate the extracellular resistivity:

$$R_{ex} = \frac{i_{post}\, 8\pi h}{c_{cl}^2\, v''_{pre}} \qquad \text{(B3.3)}$$

This equation holds as long as the cleft currents dissipate resistively and the contribution of voltage-gated currents are negligible.

Question B4. What are the relations for a finger-like synapse?

We assume a sheet-like synapse with a cleft height *h*, a constant width of 2*r*, and a length *L* that is closed at the longitudinal ends. Any current that enters the synaptic cleft cannot escape along the longitudinal axis, leaving only the transversal route to the interstitial space. Examples of such synapses are finger-like synapses, such as the neuromuscular junction or the endbulb of Held synapse for which we ignore the longitudinal endings, or deeply-invaginating, cylindrical synapses (spinules) with a circular longitudinal axis (*i.e.* a rolled-up sheet forming a cylinder). Because of the constant width, the voltage profile will be identical along the longitudinal axis, varying only along the synapse width. The capacitive current will be equal to $i_{cap}(x) = C_m v'_{pre} drdl$ (B4.1).

The current density *J* at each location will be:

$$J(x) = \frac{i(x)}{A_{esc}(x)} = \frac{C_m v'_{pre} xdl}{hdl} = \frac{C_m v'_{pre}}{h} x \qquad \text{(B4.2)}$$

The voltage gradient then is:

$$-\frac{dv(x)}{dx} = R_{ex}J(x) = \frac{R_{ex}C_m v'_{pre}}{h}x \qquad \text{(B4.3)}$$

And the voltage at x is:

$$v(x) = -\frac{R_{ex}C_m v'_{pre}}{h}\int_x^r (x)dx = \frac{R_{ex}C_m v'_{pre}}{2h}(r^2 - x^2) \qquad \text{(B4.4)}$$

The changes in the cleft potential will generate a postsynaptic, capacitive current. To calculate the total current from the finger-like synapse, we sum the current along the two dimensions:

$$i_{fin} = \int_{l=0}^{L} 2\int_{x=0}^{r} i_{cap}(x)dx\,dl = \int_{l=0}^{L} 2\int_{x=0}^{r} C_m A v'(x)dx\,dl$$

$$= \int_{l=0}^{L} 2\int_{x=0}^{r} C_m \frac{R_{ex}C_m v''_{pre}}{2h}(r^2 - x^2)dx\,dl = \frac{R_{ex}C_m^2 v''_{pre}}{h}\int_{l=0}^{L}\int_{x=0}^{r}(r^2 - x^2)dx\,dl$$

$$= \frac{R_{ex}C_m^2 v''_{pre}}{h}\int_{l=0}^{L}\left[xr^2 - \frac{1}{3}x^3\right]_{x=0}^{r} dl = \frac{2R_{ex}C_m^2 v''_{pre}r^3}{3h}\int_{l=0}^{L} dl$$

$$= \frac{2R_{ex}C_m^2 v''_{pre}r^3 L}{3h} \qquad \text{(B4.5)}$$

For the sheet-like synapse, x=0 indicates the cleft center and currents can run in two, transversal directions. We therefore multiply the capacitive current by 2 at the start of the derivation of B4.5. For a spinule synapse, no current can escape from the 'deep' end of the cylinder (at x=0) and therefore the currents run in a single, transversal direction. The right-hand side of B4.5 should therefore be halved for spinule-like synapses or other deeply-invaginating synapses, neglecting any contribution from the cup-shaped cleft at the deep end. The characteristic difference between the radial-like or sheet-like synapse is whether the escape area along the longitudinal axis increases or stays constant, respectively. Following the logic outlined in B1, B2 and B4, one can calculate the cleft potentials and postsynaptic currents for other synaptic geometries.

Question B5. How does fenestration change the cleft potential and the VC prespike?

To assess the impact of fenestration on the cleft potential and the VC prespike, we compare a radially-symmetric synapse and a synapse with *n* equally-sized fingers. The relative cleft potential can be calculated using equation B1.5 for the radially-symmetric synapse (v_{sym}) and equation B4.4 for the finger-like synapse (v_{fin}), while assuming that the cleft potential of each finger is independent from each other:

$$\frac{v_{fin}}{v_{sym}} = \frac{{r_{fin}}^2 R_{ex} C_m {v'}_{pre}(1 - x^2/r_{fin}^2)}{2h} \frac{4h}{r_{sym}^2 R_{ex} C_m {v'}_{pre}(1 - x^2/r_{sym}^2)}$$

$$= \frac{2r_{fin}^2(1 - x^2/r_{fin}^2)}{r_{sym}^2(1 - x^2/r_{sym}^2)} \qquad \text{(B5.1)}$$

This gives at the center (x=0) a ratio of:

$$\frac{v_{fin}}{v_{sym}} = 2\left(r_{fin}/r_{sym}\right)^2 \qquad \text{(B5.2)}$$

To compare the VC prespike of a radially-symmetric synapse and a fenestrated synapse, we assume that the currents from each finger are synchronized and that they sum linearly. We use equation B2.2 and equation B4.5:

$$\frac{n\, i_{fin}}{i_{sym}} = \frac{2nR_{ex}C_m^2 {v''}_{pre} r_{fin}^3 L}{3h} \frac{8h}{\pi R_{ex} C_m^2 {v''}_{pre} r_{sym}^4} = \frac{16nLr_{fin}^3}{3\pi r_{sym}^4} \qquad \text{(B5.3)}$$

We assume that the total contact surface is conserved, so the surface of the fenestrated synapse ($n\ 2r_{fin}\ L$) and the radially-symmetric synapse (πr_{sym}^2) should be equal. Therefore $L = \pi r_{sym}^2 (n\ 2r_{fin})^{-1}$, which we insert into equation B5.3:

$$\frac{n\, i_{fin}}{i_{sym}} = \frac{16nr_{fin}^3\, \pi r_{sym}^2}{3\pi r_{sym}^4\ n\ 2r_{fin}} = \frac{8}{3}\left(r_{fin}/r_{sym}\right)^2 \qquad \text{(B5.4)}$$